Journal of Asian Earth Sciences 266 (2024) 106134

Contents lists available at ScienceDirect

Journal of Asian Earth Sciences

journal homepage: www.elsevier.com/locate/jseaes

Revisiting the depositional age and provenance characteristics of metasedimentary rocks from the basement units in the Central Pontides (N Turkey): New constraints for tectonic evolution of the southern Black Sea region

Okay Çimen [a,*], Mehmet Ali Gücer [b], Cüneyt Akal [c], Mehmet Cemal Göncüoğlu [d], Mehmet Arslan [e], Antonio Simonetti [f], Fatih Karaoğlan [g,h]

[a] Munzur University, Department of Geography, Tunceli, Turkey
[b] Gümüşhane University, Department of Geological Engineering, Gümüşhane, Turkey
[c] Dokuz Eylül University, Department of Geological Engineering, İzmir, Turkey
[d] Middle East Technical University, Department of Geological Engineering, Ankara, Turkey
[e] Karadeniz Technical University, Department of Geological Engineering, Trabzon, Turkey
[f] University of Notre Dame, Department of Civil and Environmental Engineering and Earth Sciences, Notre Dame, IN, USA
[g] Çukurova University, Department of Geological Engineering, Adana, Turkey
[h] Department of Geological Processes, Institute of Geology, The Czech Academy of Sciences, Prague, Czech Republic

ARTICLE INFO

Keywords:
Whole rock geochemistry
Detrital zircon U-Pb and trace element systematics
Ar-Ar dating
Hf isotope data
Basement units of the Central Pontides
Black Sea region

ABSTRACT

The pre-Jurassic tectonic evolution of the Central Pontides in northern Turkey is still poorly understood due to the lack of detailed geochemical and geochronological data from the basement units. Therefore, this study reports for the first time combined whole rock geochemistry, trace element data and U-Pb ages for detrital zircons, and Ar-Ar geochronological data from the metasedimentary rocks of the Devrekani Massif, Geme Complex, and the Serveçay Unit to better understand their provenance, depositional age characteristics, and tectonic evolutions. The detrital zircon U-Pb data of metasedimentary units from the Devrekani Massif, Geme Complex, and the Serveçay Unit yield *ca.* 191, 185 and 298 Ma maximum depositional ages (youngest age peaks), respectively. The Devrekani Massif is dominated by Permo-Carboniferous-aged detrital zircons (67 %), whereas Neoproterozoic and Devonian-aged detrital zircons are more common in the Geme Complex (47 %) and the Serveçay Unit (53 %). These distinct age distributions clearly indicate that the Devrekani Massif may has been deposited in a dissimilar location compared to the Geme Complex and the Serveçay Unit. Furthermore, in contrast to the Devrekani Massif, the source area of the metasedimentary rocks from the Geme Complex is comparable with that of the Serveçay Unit. Lastly, the obtained detrital zircon U-Pb and mica Ar-Ar ages suggest that the Devrekani Massif and the Geme Complex were deposited and metamorphosed during the Early and Middle Jurassic, respectively. The Serveçay Unit was deposited and metamorphosed in the Permian.

1. Introduction

Clastic sedimentary rocks may provide important information with regards to depositional environment and provenance since they are composed of mineral grains and rock fragments derived from erosion of source rocks (e.g., Cullers, 1995; Armstrong-Altrin et al., 2004). Several investigative methods such as whole rock geochemistry and detrital zircon U-Pb geochronology have widely been applied and deemed effective in deciphering the tectonic evolution of clastic rocks and paleogeographical reconstruction of ancient-to-modern basins in different tectonic settings (e.g., Akdoğan et al., 2019; Ustaömer et al., 2016; Löwen et al., 2017). In addition, in-situ Hf isotope and trace element characteristics of detrital zircon grains record significant information relative to crustal evolution and composition of source rocks (e.g., Wang et al., 2016 and references therein).

The Central Pontides region in northern Turkey (Fig. 1a) contains

* Corresponding author.
E-mail address: okaycimen@gmail.com (O. Çimen).

https://doi.org/10.1016/j.jseaes.2024.106134
Received 10 December 2023; Received in revised form 23 March 2024; Accepted 26 March 2024
Available online 27 March 2024

fragments of two distinct tectonic units known as the Istanbul–Zonguldak Terrane (IZT) to the north and the Sakarya Composite Terrane (SCT) to the south (e.g., Şengör and Yılmaz, 1981; Göncüoğlu et al., 2000, 2014; Okay et al., 2015, 2018). These continental fragments are separated by the Intra-Pontide Zone (IPZ), which is mainly composed of oceanic magmatic and sedimentary units (Fig. 1a, e.g., Floyd et al., 2000; Robertson and Ustaömer, 2004; Çimen et al., 2016, 2017, Özkan et al., 2020). Also, the remnants of the Izmir-Ankara-

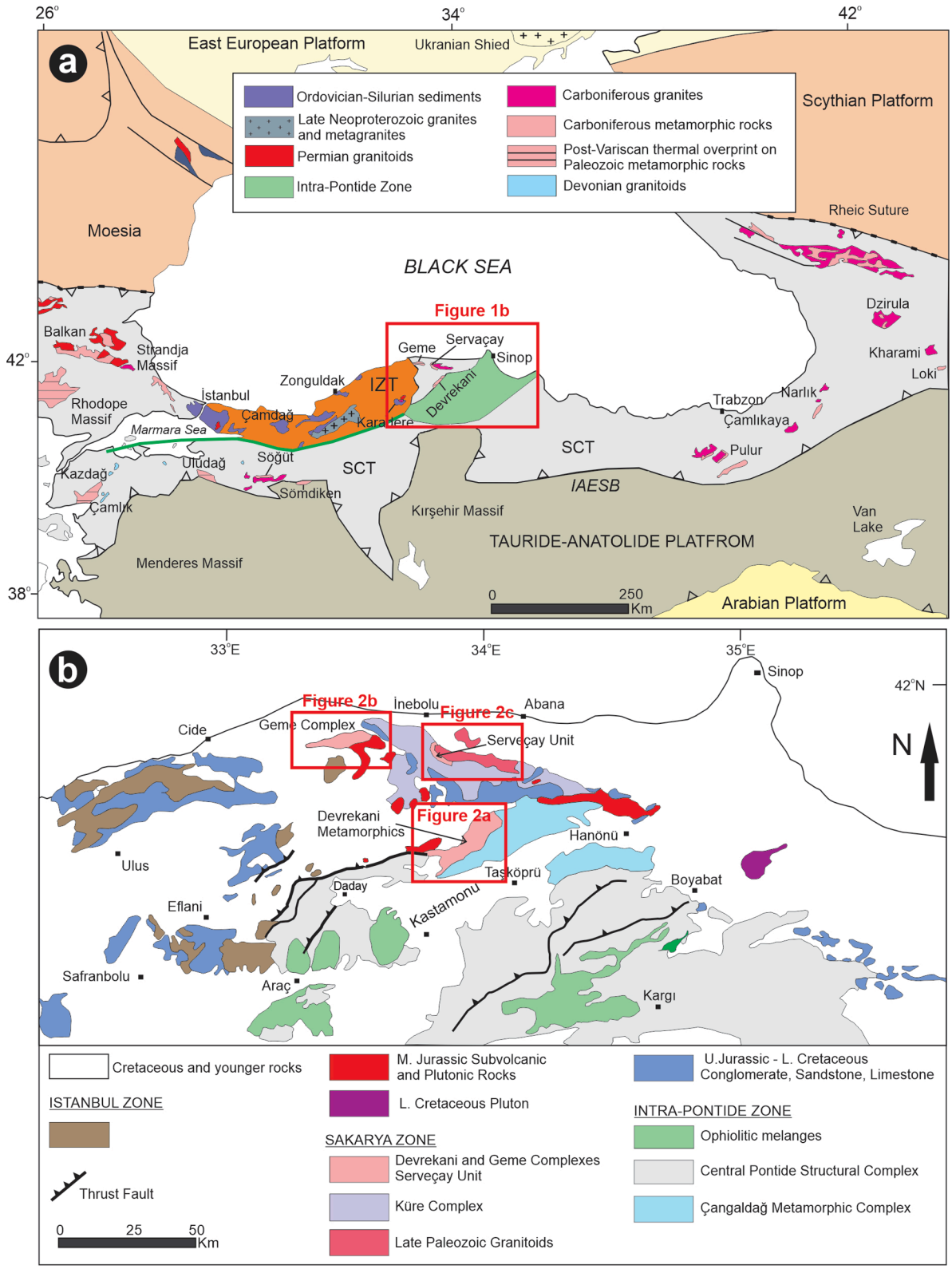

Fig. 1. (a) Tectonic map of the Black Sea region with the main alpine terranes (modified from Okay and Topuz, 2017; Çimen et al., 2017, 2018; Çimen 2020a, 2020b). SCT: Sakarya Composite Terrane. IZT: İstanbul-Zonguldak Terrane. IAESB: İzmir-Ankara-Erzincan Suture Belt. (b) Simplified geological map of the Central Pontides (modified after Göncüoğlu et al., 2014; Okay et al., 2015; Çimen et al., 2018; Çimen, 2020a, 2020b).

Erzincan Suture Belt (IAESB; Fig. 1a) are present in the south of the Central Pontides, and separate the SCT and the Tauride-Anatolide Platform (TAP) (e.g., Çelik et al., 2011; Robertson et al., 2014, Mueller et al., 2019).

There remains a lack of consensus on the geological evolution of the Central Pontides, which represents a crucial area to understand the tectonic development of northern Turkey and the southern Black Sea region (Fig. 1a). Even though the post-Triassic evolution of the region is relatively well-understood, its pre-Jurassic history is still under debate (e.g., Okay et al., 2013; Akdoğan et al., 2017; Aygül et al., 2016; Ellero et al., 2015, 2021; Frassi et al., 2018, 2020; Çimen et al., 2018). The Central Pontides consist mainly of pre-Jurassic basement units that include the Triassic-Early Jurassic Küre Complex, the widespread Jurassic continental arc magmatics, and the post-Jurassic cover units (Fig. 1b). The pre-Jurassic basements in the region are represented by metamorphic units, such as the Devrekani Massif, the Geme Complex, and the Serveçay Unit (Fig. 1b). It has been postulated that the depositional age of protoliths for the metasedimentary rocks from these basement units is pre-Cambrian or Paleozoic (e.g., Tüysüz, 1990; Aydın et al., 1995; Boztuğ et al., 1995; Kozur et al., 2000; Nzegge, 2008; Göncüoğlu, 2010; Okay et al., 2014; Okay and Nikishin, 2015; Gücer et al., 2019; Çimen, 2020a). However, detailed geochronological data for these rock assemblages are still lacking.

Therefore, this study presents combined whole rock geochemistry, trace element and U-Pb geochronological data for detrital zircon, and Hf isotope data for the metasedimentary rocks from the Devrekani Massif, the Geme Complex, and the Serveçay Unit to better evaluate their respective depositional ages and provenance signatures. New mica Ar-Ar ages for metasedimentary rocks from the Serveçay Unit are also reported, and these are compared with those from the Devrekani Massif and the Geme Complex (Okay et al., 2014; Gücer et al., 2019) to better constrain the geological evolution of the Central Pontides.

2. Geological and petrographical characteristics

2.1. Devrekani Massif

The Devrekani Massif stretches in an NE-SW direction (2–8 km wide and 30–35 km long) and is tectonically located between the Triassic-Early Jurassic Küre Complex and the Middle Jurassic Çangaldağ Metamorphic Complex (Fig. 2a; Gücer et al., 2019). It is intruded by the Middle Jurassic Devrekani Pluton and unconformably overlain by the Upper Cretaceous-Tertiary cover units (Fig. 2a). This unit includes medium-to-high-grade metamorphic rocks such as paragneisses, amphibolites, and metacarbonates (Fig. 3a, b) that were metamorphosed under amphibolite-granulite facies conditions (e.g., Boztuğ and Yılmaz, 1995; Boztuğ et al., 1995; Ustaömer and Robertson, 1999; Gücer et al., 2016). These rock assemblages are also cut by the Permo-Carboniferous granitoids (316 ± 9 and 252 ± 9 Ma) that were deformed and subsequently metamorphosed (Gücer et al., 2019). The presence of such metagranitoids is a common feature of the Variscan basements that are present within the different regions of the SCT (Fig. 1a, e.g., Göncüoğlu, 2010; Okay and Topuz, 2016). It has been proposed that the protoliths of amphibolite, orthogneiss, and paragneiss rock assemblages in the Devrekani Massif are island-arc tholeiitic basalts, I-type calc-alkaline volcanic arc granitoids, and clastic sediments (shale-wackestone), respectively (Gücer et al., 2016).

Yılmaz and Bonhomme (1991) previously reported a Jurassic age of metamorphism (149 ± 4 Ma to 170 ± 10 Ma) based on K-Ar age determinations for mica and amphibole from paragneiss samples in the Devrekani Massif. Recently, similar Jurassic Ar-Ar mica ages of 151 ± 1 and 156 ± 2 Ma have been published by Okay et al. (2014) and Gücer et al. (2016), respectively. A total of 17 detrital zircons were dated (*ca.* 293 to 1889 Ma) from two paragneiss samples in the Devrekani Massif by Gücer (2014). This limited data already indicates an upper Permian depositional age for protoliths of the paragneiss samples. Lastly, some metaophiolite slices (Dibekdere metaophiolite, Yılmaz, 1980) that are boninitic in nature (Çimen, 2020a) are tectonically intercalated within the metamorphic rocks of the Devrekani Massif (Fig. 2a). A Middle Jurassic age of 163 ± 9 Ma was reported for a metadiorite body that intrudes a metaophiolite slice, indicating that these oceanic fragments were sliced into the Devrekani Massif prior to the Middle Jurassic (Çimen et al., 2018).

The metasedimentary rocks of the Devrekani Massif are classified into three main groups based on their mineral abundances: biotite gneisses, biotite feldspar gneisses, and quartz feldspar gneisses (Fig. 4a-

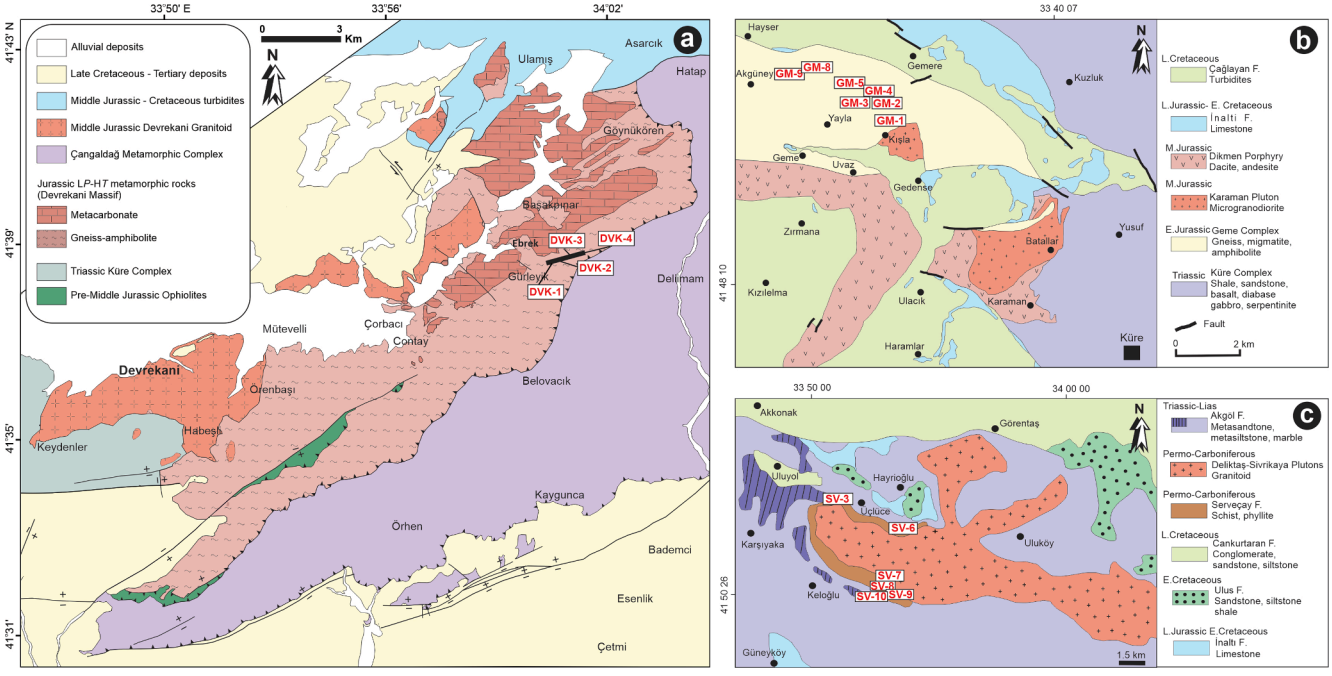

Fig. 2. Detailed geological maps of the (a) Devrekani Massif (modified after Gücer et al., 2019), (b) the Geme Complex (modified after MTA, 2002; Okay et al., 2014) and (c) the Serveçay Unit (modified after MTA, 2002) including the sampling locations (see Table 1 for sample coordinates).

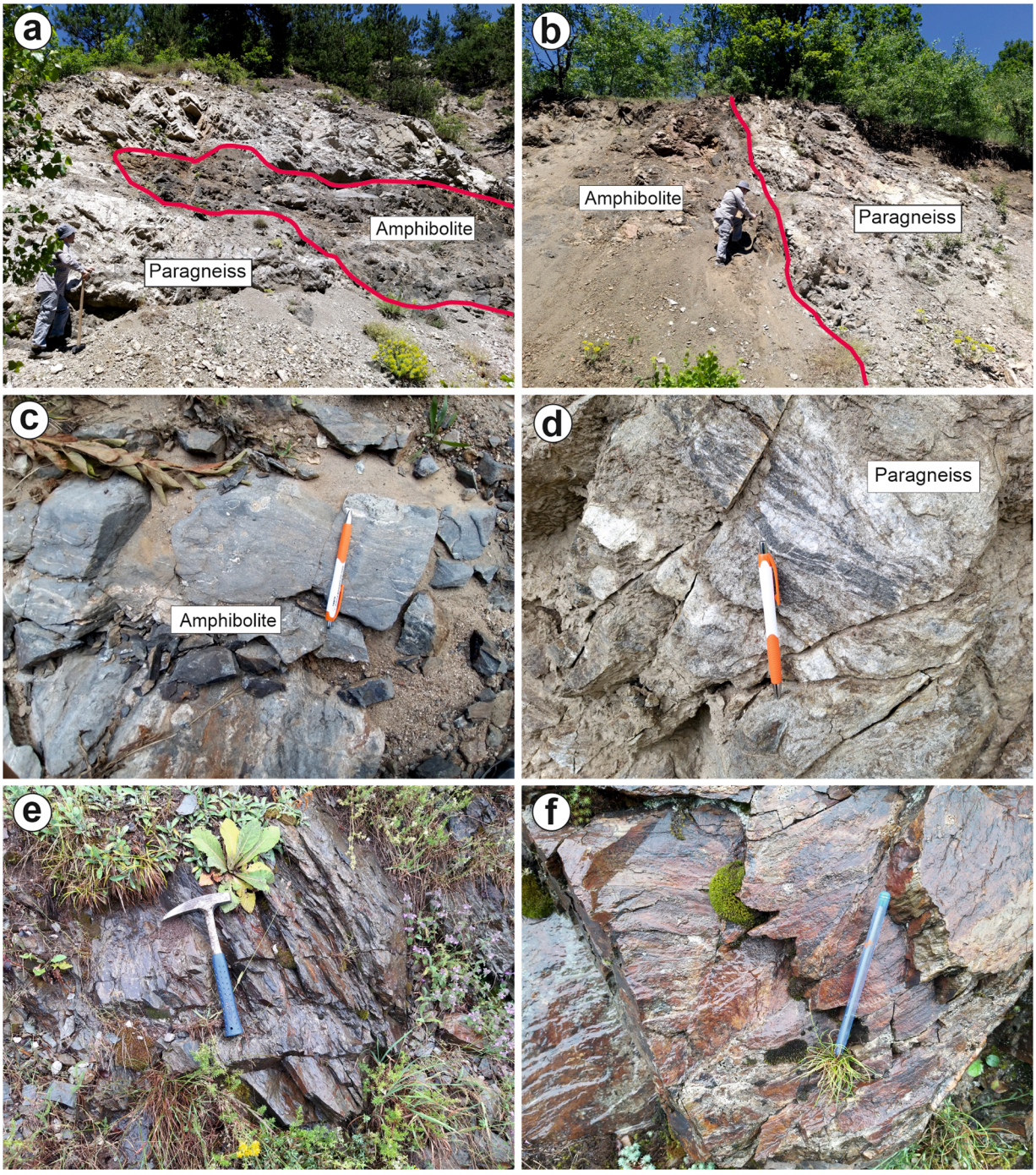

Fig. 3. **(a-b)** Field views of paragneiss and amphibolite units in the Devrekani Massif, **(c-d)** amphibolite and paragneiss units in the Geme Complex, and **(e-f)** phyllite and schist rock types in the Serveçay Unit.

c). They comprise various abundances of quartz, K-feldspar (orthoclase and/or microcline), plagioclase, biotite, and lesser secondary minerals (Table 1). Furthermore, they are weakly foliated and predominantly show lepidogranoblastic textures. Some specimens are foliated or banded with a light band composed of quartz and feldspar grains, and a band of dark-colored minerals such as biotite.

2.2. Geme Complex

The Geme Complex is in the northwest region of the Devrekani Massif (Fig. 1b) represents another basement unit of the Central Pontides. It crops out in an area of about 25 km length and 7 km width, and is cut by the Middle Jurassic Dikmen Porphyry (163 ± 4 Ma; Okay et al., 2014) and the Karaman Pluton (162 ± 4 Ma; Okay et al., 2014). It is unconformably overlain by both the Upper Jurassic-Lower Cretaceous İnaltı and Lower Cretaceous Çağlayan Formations (Fig. 2b; Okay et al., 2014). The Geme Complex is composed mainly of gneisses, amphibolites, and migmatites, and was metamorphosed under amphibolite-to-lower granulite-facies conditions (4 kbar and 720 °C) during the Middle Jurassic (161 ± 3 to 169 ± 5 Ma; Okay et al., 2014). The paragneisses represent the most common rocks in the Geme Complex, and are typically light-colored (whitish-greenish-dark gray) showing gneisssic texture. Amphibolites are also commonly observed as thin bands and lenses within the paragneisses and are distinctive with their

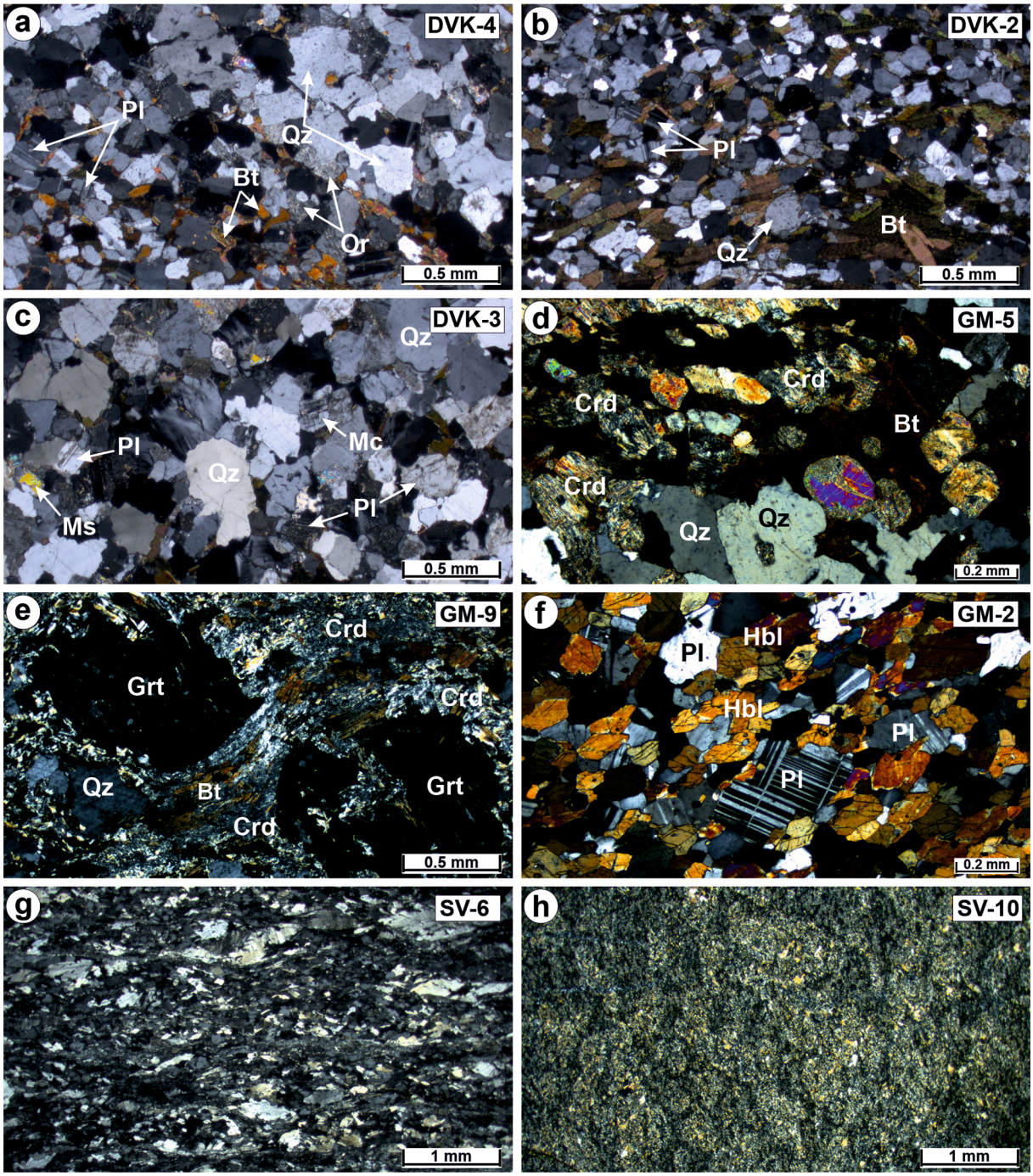

Fig. 4. Petrographic thin section images of **(a)** biotite gneiss, **(b)** biotite-feldspar gneiss, and **(c)** quartz-feldspar gneiss from the Devrekani Massif, **(d)** cordierite-biotite gneiss, **(e)** garnet-biotite-cordierite gneiss, and **(f)** amphibolite from the Geme Complex, **(g)** chlorite schist and **(h)** phyllite from the Serveçay Unit. Bt: Biotite, Crd: Cordierite, Grt: Garnet, Hbl: Hornblende, Mc: Microcline, Ms: Muscovite, Or: Orthoclase, Pl: Plagioclase, Qz: Quartz.

dark gray-greenish colors in the field (Fig. 3c, d). Of note, Okay et al. (2014) reported a paragneiss sample in this unit that is characterized predominantly by Neoproterozoic and Paleozoic and a few Paleoproterozoic and late Archean detrital zircons. Okay et al. (2014) proposed that the Geme Complex may represent the remobilized basement of the Central Pontides.

The metasedimentary rocks of the Geme Complex can be classified into four main groups based on their distinct mineral assemblages; biotite gneisses, cordierite-biotite gneisses, garnet-biotite-cordierite gneisses, and amphibolite (Table 1). These rocks mainly exhibit granoblastic, lepidogranoblastic, granonematoblastic, lepidogranoblastic, and porphyroblastic textures. Biotite and cordierite-biotite gneisses are well foliated, and the most common mineral assemblage is quartz, feldspar, biotite, and cordierite with secondary sericite and chlorite (Fig. 4d). This group of gneisses is well-foliated and contains garnet as well as biotite and cordierite as the main metamorphic minerals (Fig. 4e). Typically, these rocks exhibit granoblastic to lepidoporphyroblastic textures and contain garnet porphyroblasts with grain sizes reaching up to 2 mm. Garnet crystals are mostly present as subhedral to anhedral porphyroblasts that are fractured and fragmented. The amphibolites in the Geme Complex show banded structures of a few mm in width due to the parallel arrangement of hornblende and plagioclase crystals. The most

Table 1
Mineral assemblages of metasedimentary rocks from the Devrekani Massif, the Geme Complex and the Serveçay Unit.

Sample	Location[#]	Texture	Hbl	Ms	Qz	Pl	Kfs	Bt	Qpq	Grt	Crd	Sil	Cpx	Ep	Chl	Cal	Cld	Ser	Zr
Quartz-feldspar gneiss																			
DVK-3	0584934E 4610234 N	GB	–	⊕	++	+	++	+	+	–	–	–	–	–	*	–	–	**	⊕
Biotite schist / gneiss																			
DVK-1	0584558E 4610262 N	LGB	–	⊕	++	++	+	++	+	–	–	–	–	–	*	–	–	**	⊕
DVK-4	0585160E 4610203 N	LGB	–	⊕	++	++	++	++	+	–	–	–	–	–	*	–	–	**	⊕
GM-1	0545869E 04637947 N	GB	–	–	++	++	++	++	+	–	–	–	–	–	*	–	–	**	⊕
Biotite-plagioclase gneiss																			
DVK-2	0584813E 4610247 N	LGB	–	–	++	++	++	++	+	–	–	–	–	–	–	–	–	–	⊕
Cordierite-biotite gneiss																			
GM-5	0543277E 04640100 N	LGB	–	*	++	++	++	+	+	–	+	–	–	–	*	–	–	**	⊕
GM-8	0542665E 04640300 N	LGB	–	*	++	++	++	+	+	–	+	–	–	–	*	–	–	**	⊕
Garnet-biotite-cordierite gneiss																			
GM-9	0542577E 04640288 N	PB	–	*	++	++	++	++	+	++	++	–	–	–	–	–	–	**	⊕
Quartz-mica schist																			
SV-3	0570050E 04638126 N	LPB	–	++	++	–	–	++	+	–	–	–	–	–	*	–	–	**	⊕
SV-7	0573239E 04633962 N	LGB	–	++	++	–	–	++	+	–	–	–	–	–	+	–	–	**	⊕
SV-8	0573342E 04633772 N	LGB	–	++	++	–	–	++	+	–	–	–	–	–	*	–	–	**	⊕
SV-9	0573276E 04633485 N	LPB	–	++	++	–	–	++	+	–	–	–	–	–	+	–	–	**	⊕
Chlorite schist																			
SV-6	0574599E 04636246 N	LB	–	–	++	–	–	–	+	–	–	–	–	–	++	*	–	–	–
Phyllite																			
SV-10	0573360E 04633213 N	LB	–	–	++	–	–	–	+	–	–	–	–	–	+	–	–	++	–

++ major constituent (>%5); + minor constituent (%1–5); ⊕ accessory phase (≤%1); * secondary minerals. (from minerals and/or veins); ** secondary minerals (from feldspar and cordierite); – not observed. Hbl: Hornblende, Ms: Muscovite: Qz: Quartz, Pl: Plagioclase, Kfs: K-feldspar, Bt: Biotite, Opq: Opaques, Grt: Garnet, Crd: Cordierite, Sil: Sillimanite, Cpx: Clinopyroxene, Ep: Epidote, Chl: Chlorite, Cal: Calcite, Cld: Chloritoid, Ser: Sericite, Zr: Zircon. GB: Granoblastic, LB: Lepidoblastic, LGB: Lepidogranoblastic, LPB: Lepidoporphyroblastic, PB: Porphyroblastic. #: The locations of the samples are given in the Universal Transverse Mercator (UTM) coordinate system.

common mineral paragenesis is hornblende, plagioclase, and opaques (Fig. 4f).

2.3. Serveçay Unit

The Serveçay unit within the northern section of the Central Pontides (Fig. 1b) is mainly composed of low-to-medium grade metamorphic rocks such as schist, phyllite, mafic metatuff, metadiabase, and meta-carbonate (Kozur et al., 2000; Okay et al., 2014). It is intruded by the Permo-Carboniferous Sivrikaya (298 ± 2 and 300 ± 1 Ma) and Deliktaş (295 ± 1 Ma) granitoids, and tectonically overlain by the Triassic-Lower Jurassic Küre Complex (Fig. 2c; Nzegge, 2008; Okay et al., 2014). The phyllites typically display dark grayish-greenish color tones, whereas the schists are characterized by relatively lighter colors in the field (Fig. 3e, f). The Zirveçay Valley to the south of Gemiciler Village, can be considered as host of the type locality for the unit. While Aydın et al. (1995) considered this unit as a part of the Triassic Küre Complex, Kozur et al. (2000) proposed that it may represent another Variscan basement remnant within the Central Pontides. In addition, Aydın et al. (1995) reported a Carboniferous K-Ar age of 311.0 ± 6.2 Ma for the Serveçay Unit.

The metasedimentary rocks of the Serveçay Unit are dominated by schists and lesser amounts of phyllites. Schists are classified as quartz-mica and chlorite schists (Table 1). These rocks are well-foliated and fine-to-medium-grained, with lepidoblastic, lepidogranoblastic, and lepidoporphyroblastic textures. Quartz, muscovite, chlorite, and biotite are the main mineral components with secondary calcite and clay minerals are observed (Fig. 4g, h). Quartz- and mica-rich sections in schists show compositional layering (S0) related to the bedding of the protoliths. Asymmetrical cleavages are observed in very fine-grained quartz-mica schists, and in some specimens, horizontal compositional layering (S1) and S2-S3 deformations can be observed.

3. Analytical methods

Whole rock geochemical analyses of seventeen metasedimentary rocks reported here were conducted at the ACME laboratory in Canada. The samples were first crushed using a jaw crusher until they were reduced to small chips measuring 0.1–1 cm in size. Next, a mild-steel mill was used to powder the chips. Samples were prepared using 0.2 g of rock powder that was fused with 1.5 g of $LiBO_2$. The difference in weight before and after ignition at 1000 °C is reported as Loss on Ignition (LOI). Subsequently, samples were dissolved in 100 ml of 5 % HNO_3 in preparation for major and trace element analysis. The determination of both major and trace element compositions was conducted using inductively coupled plasma atomic emission spectroscopy (ICP-AES). The detection limits for major oxides were approximately 0.01 to 0.1 wt %, whereas for trace elements these were 0.1 to 10 ppm. Rare earth elements (REE) analysis involved using 0.25 g of rock powder that was dissolved via several acid digestion steps. Inductively coupled plasma mass spectrometry (ICP-MS) was used to analyze the REEs and the detection limits ranged from 0.01 to 0.5 ppm.

In-situ U-Pb age determinations and rare earth element (REE) concentrations for individual zircon grains retrieved from metasedimentary rocks were conducted using a Perkin-Elmer Nexion2000P ICP-MS instrument coupled to a NWR213 nm laser ablation system at Central Research Laboratory, Çukurova University (Turkey). After heavy mineral separation and hand-picking of crystals using a binocular stereomicroscope, zircon grains were embedded on glass slides and polished to reveal their internal structure. The cathodoluminescence (CL) imaging of zircon grains was conducted at HUNITEK Laboratory located in Hacettepe University, Turkey using a Tescan GAIA 3 instrument, which is a scanning electron microscope equipped with a focused ion beam. Details for laser ablation parameters and conditions employed are described in Sapancı et al. (2023). Plešovice (Sláma et al., 2008), 91,500 (Wiedenbeck et al., 1995) and GJ1 (Horstwood et al., 2016) reference zircons were used to validate and ensure the accuracy of the laser ablation analyses. Finally, the data were imported into the Excel-based macro IsoPlot 4.15 (Ludwig, 2012) to perform the relevant calculations and generate concordia diagrams.

In-situ Lu-Hf isotope analyses for selected zircon grains were conducted at the Nanjing FocuMS Technology Co. in China using a LA-MC-ICP-MS instrument configuration, which consists of a193 nm ArF *RESOlution LR* laser-ablation system (Australian Scientific Instruments, AU) and a *Nu Plasma II* MC-ICP-MS (Nu Instruments, UK). Laser ablation analyses were conducted with a fluence of 4.5 J/cm^2 focused on the zircon surface. Each individual acquisition involved a 20 s gas blank background measurement, followed by lasering using a spot diameter of 50 μm and a 9 Hz repetition rate for 40 s. A helium flow rate of 370 ml/min was applied as the carrier gas to efficiently transport aerosol out of the ablation cell, and was mixed with argon at about 0.97 L/min via T-connector before entering ICP torch. An integration time of 0.3 s was employed for ion signal acquisition equating to 133 cycles during the 40 s laser ablation period. During each analytical session, for data verification and quality control purposes of measured Hf isotope ratios, three reference zircons, including GJ-1 (Yuan et al., 2008), 91,500 (Wu et al., 2006; Yuan et al., 2008), Plešovice (Sláma et al., 2008), Mud Tank (Griffin et al., 2006; Yuan et al., 2008), and Penglai (Li et al., 2010) were alternatively ablated for, every 15 unknown zircon grains.

Muscovite crystals from two metasedimentary samples (SV-3 and −6) from the Serveçay Unit were dated at the ^{40}Ar-^{39}Ar and Noble Gas Laboratory in the STEM Faculty at the Open University (UK). The infrared (IR) laser probe spot dating technique was used to analyze muscovite crystals, and details for analytical procedures employed for this study are described in Supplementary Table S5.

4. Results

4.1. Whole rock geochemistry

Major and trace element concentrations obtained for the metasedimentary rocks from the Devrekani Massif, Geme Complex, and Serveçay Unit are reported in Table 2. As stated earlier, all samples investigated here were metamorphosed between low and high-grade metamorphic conditions (Aydın et al., 1995; Okay et al., 2014; Gücer et al., 2019), and therefore, immobile trace elements (e.g., high field strength elements, HFSEs and REEs) were used solely for geochemical and provenance interpretations. Consequently, mobile elements (e.g., large ion lithophile elements, LILEs) were excluded from the geochemical diagrams presented here since they may have been remobilized during the various metamorphic events (e.g., Floyd and Winchester, 1978; Pearce and Cann, 1973).

According to the source area classification diagram (Fig. 5a; Floyd and Leveridge, 1987), the samples from the Devrekani Massif, Geme Complex, and Serveçay Unit are mainly characterized by low La/Th values (1.85 to 4.12) and high Hf (3 to 7 ppm) contents and plot proximal to the field for an acidic arc source region. In the source rock classification diagram (Fig. 5b; McLennan et al., 1993), the samples investigated here mainly display similar Co/Th (0.16 to 2.64) and La/Sc (1.25 to 3.61) values and fall within the felsic volcanic rocks field. Of note, one sample (DVK-1) from the Devrekani Massif is characterized by a higher La/Sc (6.85) value compared to those from other samples, and most of the samples from the Serveçay Unit display higher Co/Th values than those from both the Devrekani Massif and the Geme Complex (Fig. 5b).

In the tectonic setting discrimination diagrams (Fig. 5c, d; Bhatia and Crook, 1986), Ti/Zr (10.37–33.52), La (11.4–44.8 ppm), Th (4.1–22.2 ppm), Sc (4–21 ppm) and Zr/10 (9.5–32) values for samples reported here are consistent with those from continental arc and active continental margin settings. Here, the samples from the Devrekani Massif mostly plot in the active continental margin field, whereas the samples from the Geme Complex and the Serveçay Unit mainly fall within the continental arc field.

Based on the chondrite-normalized REEs patterns (Fig. 5e; Boynton, 1984), the samples from the basement units reported here are characterized by enrichments in light LREEs relative to heavy REEs (La_N/Yb_N = 5.31–13.13) and associated with negative Eu-anomalies (EuN/Eu*= 0.51–0.91). In this diagram, one sample (GM-1) from the Geme Complex displays a more depleted REE pattern compared to those from other samples. In the primitive mantle (PM)-normalized multi-element diagram (Fig. 5f; Sun and McDonough, 1989), the samples are characterized by enriched elemental patterns relative to PM (e.g., ThN = 48.24–261.18; LaN = 16.59–65.21; N: PM-normalized) coupled with negative Nb (5.33–28.05), Ta (4.88–58.54), P (0.46–20.67) and Ti (1.48–4.66) anomalies, and these multi-element patterns are consistent with those for samples derived from an upper crustal source (Fig. 5f; Rudnick and Gao, 2003).

4.2. Detrital zircon u-pb ages

A combined total of > 1000 zircon grains were extracted from the metasedimentary samples within the Devrekani Massif, the Geme Complex, and the Serveçay Unit, and have been investigated for their corresponding U-Pb ages by conducting in-situ LA-MC-ICP-MS analyses. A total of 851 zircons yielded concordant zircon ages (at 90–110 % level; Fig. 6 and Table S1), and therefore only these ages were used to better evaluate the depositional age and provenance characteristics of the basement units. The zircons exhibit mainly short to long prismatic, subhedral-to-rounded forms with oscillatory zoning and fracturing. Their sizes range between 30 and 360 μm with length/width ratios of approximately 2:1.

A total of 293 zircon grains from four metasedimentary samples (paragneiss, DVK1-2–3 and −4) in the Devrekani Massif yielded concordant ages ranging from 2271 Ma (Paleoproterozoic) to 184 Ma (Early Jurassic) and are mainly Paleozoic-aged (n = 256, 88 %; Figs. 6 and 7a; Table S1). Most of the zircon ages for the Devrekani metasedimentary rocks are Carboniferous (n = 142, 48 %), Permian (n = 55, 19 %) and Devonian (n = 31, 11 %), characterized by ages of 270 Ma, 310 Ma and 340 Ma, and a lesser number of 490 Ma and 560 Ma age peaks are noted (Fig. 7a, b). The other age populations are Neoproterozoic (n = 21, 7 %), Cambrian (n = 15, 5 %), Ordovician (n = 8, 3 %), Triassic (n = 10, 3 %), Silurian (n = 5, 2 %) and Paleoproterozoic (n = 2, 1 %). The youngest zircon age (184 ± 13 Ma) and the youngest peak age (n = 5, 1 %, 191.0 ± 4.9 Ma; Dickinson and Gehrels, 2009) indicate an Early Jurassic maximum depositional age for protoliths of the metasedimentary rocks from the Devrekani Massif (Fig. 7b).

In total, 249 concordant ages were obtained from four metasedimentary samples (paragneiss, GM1-5–8 and −9) in the Geme Complex (Figs. 6 and 8a; Table S1), and these ages vary from 3279 Ma (Archean) to 182 Ma (Early Jurassic) and mainly include Paleozoic (n = 111, 45 %) and Neoproterozoic (n = 81, 33 %) ages. A majority of the Paleozoic ages are Devonian (n = 34, 14 %) and Carboniferous and Permian (total n = 36, 14 %). The remainder of the Paleozoic age groups are Silurian (n = 16, 7 %), Ordovician (n = 13, 5 %) and Cambrian (n = 11, 4 %). Apart

Table 2
Representative whole-rock geochemical composition of the basement units of the Central Pontides (N Turkey).

Sample	DVK-1	DVK-2	DVK-3	DVK-4	SV-3	SV-6	SV-7	SV-8	SV-9
Locations	Devrekani Massif				Serveçay Unit				
SiO_2	70.19	57.82	70.55	61.04	67.07	62.43	55.21	65.95	70.79
Al_2O_3	14.91	19.06	14.81	18.14	16.07	19.38	21.58	15.87	13.16
Fe_2O_3*	3	6.12	2.74	4.83	5.25	5.73	8.42	6.52	5.63
MgO	1.44	2.34	1.26	2.75	2.2	1.7	2.68	1.9	1.87
CaO	1.24	3.84	1.79	2.86	0.38	0.07	0.17	0.23	0.14
Na_2O	4.51	5.09	3.96	3.67	0.81	0.77	1.64	1.71	2.27
K_2O	3.28	2.91	3.38	3.98	3.45	4.68	4.11	2.61	1.75
TiO_2	0.32	0.82	0.32	0.71	0.68	0.75	1.01	0.81	0.74
P_2O_5	0.1	0.45	0.09	0.08	0.09	0.04	0.11	0.1	0.09
MnO	0.07	0.14	0.07	0.14	0.09	0.07	0.1	0.07	0.07
Cr_2O_3	0.003	<0.002	0.002	0.01	0.011	0.013	0.016	0.012	0.009
LOI	0.8	1.2	0.9	1.6	3.7	4.1	4.7	4	3.3
Sum	99.88	99.82	99.91	99.83	99.86	99.87	99.83	99.87	99.88
Ba	376	306	347	634	754	913	648	387	304
Sc	6	7	7	11	14	19	21	15	15
Be	7	bdl	7	3	3	1	bdl	bdl	1
Co	3.5	7.3	4.5	9.4	11.3	6.2	16	13.1	13.5
Cs	5.5	8.2	2.5	8.8	5.5	4.5	3.3	2.4	1.8
Ga	19.1	25	18.4	24.6	19.6	25.5	25.5	18.5	14.5
Hf	5.1	7	3	5.3	4.8	3.6	5.1	4.6	4.9
Nb	20	17.2	14	13.6	9.1	10.9	14.1	10.1	8
Rb	181.4	217.3	115.7	162.1	132.4	139.7	126.4	76.1	54.1
Sn	9	7	3	12	1	2	2	1	1
Sr	65.4	263.8	105.7	171.6	86.6	45.5	46.6	64.1	46.7
Ta	2.4	2.4	1.8	1	0.7	0.6	0.8	0.7	0.6
Th	22.2	6.8	9.2	19	9	9.6	11.4	8.3	6.8
U	7.5	4.7	2.7	5.7	3.1	3.7	3.8	2.7	2
V	27	45	37	73	104	135	160	109	113
W	3.2	1.6	3.6	8.6	1.5	3	2.4	2.5	1.2
Zr	184.9	320.3	95	198.9	180.7	132.1	187	179.5	178.7
Y	22.8	30.2	20.6	25.7	16.6	15.3	21.6	25.1	19.9
La	41.1	25.3	18.3	36.2	29.1	23.8	27.4	34.2	25.8
Ce	78.5	50.5	36.5	69.8	45.9	48.4	54.5	69.7	52.9
Pr	8.77	5.96	4.03	7.47	6.36	4.94	6.14	7.76	5.69
Nd	31.7	24.3	14.7	26.8	24.1	17.9	23	30.2	21.6
Sm	5.99	5.11	3.18	5.51	4.57	3.41	4.51	6.06	4.17
Eu	0.93	1.26	0.57	1.01	0.95	0.88	1.01	1.27	1.02
Gd	5.2	5.05	3.15	5.02	3.75	3.29	4.01	5.27	3.99
Tb	0.81	0.86	0.56	0.79	0.57	0.53	0.63	0.87	0.64
Dy	4.22	5.15	3.42	4.5	3.23	2.97	3.58	5.28	3.55
Ho	0.76	1.08	0.71	0.88	0.66	0.56	0.83	0.93	0.73
Er	2.09	3.32	2.07	2.72	1.99	1.76	2.61	2.83	2.16
Tm	0.31	0.51	0.32	0.4	0.29	0.25	0.4	0.4	0.32
Yb	2.11	3.21	2.13	2.75	1.95	1.87	2.84	2.77	2.06
Lu	0.32	0.51	0.34	0.43	0.3	0.29	0.47	0.38	0.3
Mo	0.8	0.5	0.9	1.8	0.8	1.2	0.3	0.8	0.6
Cu	12.8	7.2	8.2	25.2	29.5	48.6	27.6	29.9	33.3
Pb	5.2	1.7	2.7	9.4	11.4	8.3	6.9	8.5	8.1
Zn	80	105	36	114	78	70	108	82	61
Ni	6.7	3.3	7.7	24.6	25.6	18.7	54.6	37.4	26.8

Sample	SV-10	GM-1	GM-2	GM-3	GM-4	GM-5	GM-8	GM-9
Locations	Serveçay Unit	Geme Complex						
SiO_2	59.47	88.87	46.88	49.28	50.31	61.06	61.99	55.87
Al_2O_3	19.5	4.3	15.77	15.93	15.22	17.66	17.35	19.81
Fe_2O_3*	7.12	3	10.69	8.9	10.91	7.65	7.45	8.49
MgO	2.67	0.76	9.05	6.33	6.07	3.09	2.78	3.79
CaO	0.15	0.07	9.44	11.1	9.54	0.56	2.12	1.65
Na_2O	1.16	0.8	3.41	3.72	4.07	2.09	2.63	0.91
K_2O	3.8	0.48	0.3	0.72	0.63	2.74	2.69	3.85
TiO_2	0.92	0.45	1.81	1.19	1.49	0.98	0.92	0.9
P_2O_5	0.11	0.01	0.13	0.08	0.12	0.08	0.11	0.08
MnO	0.06	0.03	0.18	0.18	0.19	0.13	0.12	0.36
Cr_2O_3	0.016	0.034	0.046	0.04	0.031	0.021	0.015	0.02
LOI	4.8	1.1	2	2.3	1.2	3.7	1.6	4
Sum	99.85	99.94	99.72	99.78	99.78	99.83	99.84	99.78
Ba	424	43	92	112	116	430	400	394
Sc	20	4	36	27	33	19	18	21
Be	1	bdl	1	1	3	1	bdl	bdl
Co	17.3	7.2	38	32.2	38.3	20.3	17.7	26.5
Cs	5	0.6	1	2.4	0.5	3.4	5.5	5.2
Ga	23.6	4.8	15.2	13.4	15.8	20.7	20.3	24.6
Hf	4.3	4.8	3.2	2.1	2.7	5.1	4.4	4.9

(*continued on next page*)

Table 2 (*continued*)

Sample	SV-10	GM-1	GM-2	GM-3	GM-4	GM-5	GM-8	GM-9
Nb	11.6	3.8	2.7	1.1	1.9	10.6	9.6	16
Rb	109.2	16.8	5.5	18.9	7.8	87.3	91.1	140.2
Sn	2	1	bdl	1	bdl	1	2	1
Sr	42.9	15	270	348.3	214.8	100.2	155.9	93.1
Ta	0.8	0.2	0.2	bdl	bdl	0.6	0.6	0.8
Th	10	4.1	0.5	0.4	0.9	8.9	6.7	15.6
U	2.9	0.5	bdl	0.4	0.3	3	2.7	1.9
V	148	51	263	182	254	140	124	173
W	2.2	0.8	bdl	0.8	bdl	0.8	1.5	bdl
Zr	151.2	179.2	125.8	75.2	106.5	182.8	164.5	181.2
Y	23.1	5.9	31.2	22.8	30.2	27.5	25.2	26.4
La	35.8	11.4	6.7	3.6	6.5	32.7	23.6	44.8
Ce	71.2	22.4	17.3	10.5	15.5	64.7	49.1	100.9
Pr	7.78	2.24	2.63	1.66	2.34	7.45	5.63	9.58
Nd	28.4	8.5	13.3	8.7	12	28.9	22.4	36.5
Sm	4.77	1.51	3.94	2.71	3.85	5.64	4.75	6.52
Eu	1.26	0.31	1.39	1.02	1.23	1.36	1.39	1.03
Gd	4.24	1.32	5.41	3.66	4.91	5.23	4.63	5.66
Tb	0.73	0.19	0.95	0.65	0.87	0.85	0.78	0.88
Dy	4.44	1.04	6.13	4.04	5.66	5.12	4.84	4.99
Ho	0.88	0.23	1.24	0.87	1.15	1.03	0.94	0.93
Er	2.82	0.72	3.56	2.45	3.49	3.24	2.74	2.81
Tm	0.41	0.1	0.51	0.35	0.47	0.44	0.41	0.43
Yb	2.83	0.68	3.14	2.23	3.17	3.04	2.65	2.81
Lu	0.44	0.11	0.49	0.34	0.46	0.48	0.39	0.43
Mo	0.2	1.4	0.3	0.4	0.2	0.5	1	0.7
Cu	19.3	26	42.6	14.1	18.6	40.9	26	168.8
Pb	3.8	1.4	1.1	5.6	4.6	8.8	3.5	3.7
Zn	63	15	25	38	32	81	67	95
Ni	67.8	61.5	79	39.3	26.6	80.2	56.3	104.4

LOI: Loss on ignition, bdl: below detection limit

from the Neoproterozoic age group mentioned above, there are also Archean (n = 20, 8 %), Paleoproterozoic (n = 18, 7 %) and Mesoproterozoic (n = 12, 5 %) age groups in the detrital zircons from these rocks (Fig. 8a). Moreover, they display mainly 340 Ma, 392 Ma, 430 Ma and 600 Ma and lesser 260 Ma and 503 Ma age peaks, and the youngest zircon age (182 ± 8 Ma) and the youngest peak age (n = 3, 185.0 ± 2.3 Ma; Dickinson and Gehrels, 2009) suggest an Early Jurassic maximum depositional age (Fig. 8b). Furthermore, the zircon grains extracted from an amphibolite sample (GM-4) that is interlayered with metasedimentary units in the field yielded an age of 191 ± 5 Ma (Fig. 6d), which confirm the presence of Early Jurassic depositional age for this unit.

Analyses of 310 detrital zircon grains from six metasedimentary samples (schist and phyllite, SV3-6–7-8–9 and −10) from the Serveçay Unit yielded concordant ages (Figs. 6 and 9a; Table S1) ranging from 3098 Ma (Archean) to 195 Ma (Early Jurassic). These age populations are mostly characterized by the presence of pre-Cambrian zircons (n = 156, 50 %) comprising Neoproterozoic (n = 113, 37 %), Paleoproterozoic (n = 23, 7 %), Archean (n = 12, 4 %) and Mesoproterozoic (n = 8, 3 %) ages (Fig. 9a). The remaining age groups are Devonian (n = 49, 16 %), Silurian (n = 35, 11 %), Ordovician (n = 31, 10 %), Carboniferous (n = 17, 5 %), Cambrian (n = 14, 5 %) and Permian (n = 6, 2 %). In addition, the main age peaks are 425 Ma and 610 Ma in the detrital zircon grains reported here (Fig. 9b), and the youngest peak age (n = 8, *ca.* 298 to 280 Ma; Dickinson and Gehrels, 2009) indicate an early Permian maximum depositional age for the Serveçay Unit (Fig. 9b).

4.3. Detrital zircon trace element data

Zircon grains from the metasedimentary rocks (paragneiss, DVK1-2–3 and −4) of the Devrekani Massif have U/Yb ratios of 0.07–1.24, Hf- and Y-concentrations of 6296–13148 ppm and 372–6881 ppm, respectively, and these values plot mainly in the continental zircon field rather than the oceanic zircon field (Fig. 10a, b and Table S2; Grimes et al., 2007). The metasedimentary rocks (paragneiss, GM1-5–8 and −9) of the Geme Complex are characterized by zircons that exhibit U/Yb ratios of 0.02–2.27, and Hf- and Y-concentrations of 228–15399 ppm and 174–4538 ppm, respectively. Most of these values fall into the field of continental zircons, but some of them plot in the oceanic zircon field (Fig. 10c, d and Table S2; Grimes et al., 2007). Lastly, zircon crystals obtained from the metasedimentary rocks (schist and phyllite, SV3-6–7-8–9 and −10) of the Serveçay Unit have U/Yb ratios of 0.01–2.70, and Hf- and Y-concentrations of 234–11529 ppm and 201–22682 ppm, respectively. While these values mainly plot in the continental zircon field, a few of them fall within the oceanic zircon field similar to those from the Geme Complex (Fig. 10e, f and Table S2; Grimes et al., 2007). In addition, Th/U values of zircons investigated here from the Devrekani Massif, the Geme Complex, and the Serveçay Unit vary between 0.02 and 1.74, 0.01–2.29 and 0.01–2.49, respectively (Table S3). A total of 93 % (n = 796) of zircon grains have Th/U ratios of > 0.1, which indicate that most of the zircon grains were derived from igneous rocks (mainly felsic melts) and a small portion are metamorphic in origin (Fig. S1; Rubatto, 2002; Linnemann et al., 2011). Also, it is well-documented that metamorphism overprint may cause Th-loss (e.g., Gärtner et al., 2016), and the lower Th/U ratios for zircons from the Devrekani Massif and Geme Complex may be attributed to the regional middle Jurassic metamorphism event (Okay et al., 2014; Gücer et al., 2016). Moreover, REE concentrations of zircons reported here also suggest the presence of mainly continental crust source regions (Table S2 and Fig. S2; Hoskin and Ireland, 2000; Grimes et al., 2007).

4.4. Detrital zircon Hf isotope data

Lu-Hf isotopic measurements were conducted on zircons that are characterized by ages between 820 and 579 Ma. A source region corresponding to this period is thus far only reported from the Karadere Unit of the IZT (Göncüoğlu et al., 2022). $^{176}Hf/^{177}Hf$ ratios for zircons (820 to 579 Ma; n = 55) from metasedimentary rocks (paragneiss, GM1-5 and-8) of the Geme Complex vary between 0.281788 and 0.282769, which correspond to $\varepsilon Hf_{(t)}$ values of –19.59 to + 13.94, and two-stage depleted mantle model (T_{DM2}) ages of 2841 to 710 Ma (Fig. 11 and Table S4). Similarly, zircon grains (721 to 579 Ma; n = 78) from metasedimentary rocks (schist and phyllite, SV3-6–7-8–9 and −10) of the

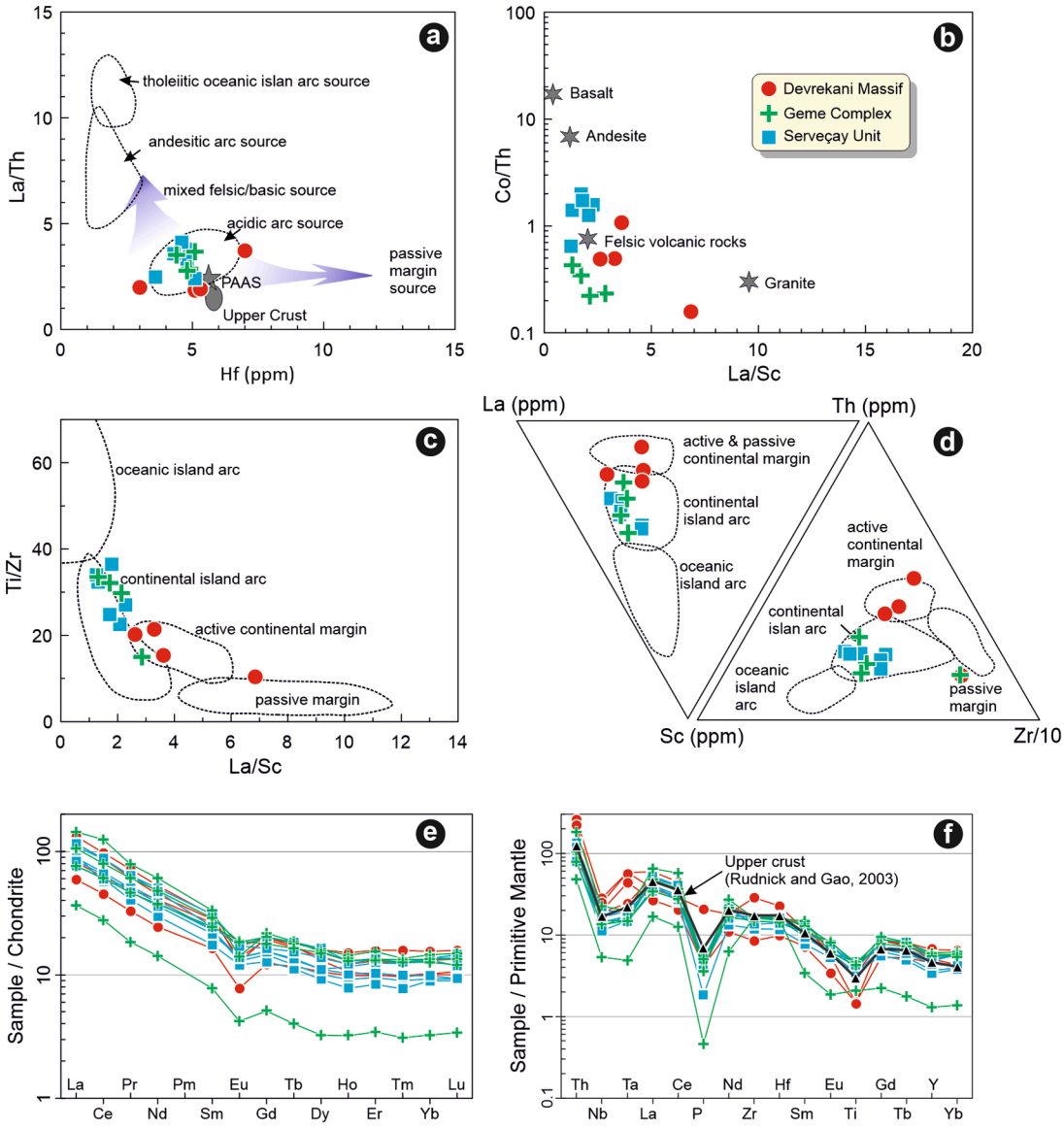

Fig. 5. (a-b) Diagrams of source rock discrimination (Floyd and Leveridge, 1987; McLennan et al., 1993), (c-d) Diagrams of tectonic setting discrimination (Bhatia and Crook, 1986), (e) Chondrite-normalized REE patterns (Boynton, 1984), (f) PM-normalized multi-element patterns (Sun and McDonough, 1989). Upper crust values are taken from Rudnick and Gao (2003).

Serveçay Unit range between 0.281417 and 0.282780, and these values correspond to εHf(t) values of –34.06 to + 14.12 and T_{DM2} ages of 3686 to 668 Ma (Fig. 11 and Table S4).

4.5. Mica ^{40}Ar-^{39}Ar ages

Okay et al. (2014) previously published ages of 146 ± 2 and 151 ± 1 Ma for biotite and muscovite grains from the metasedimentary rocks of the Devrekani Massif. Subsequently, Gücer et al. (2016) reported similar ages of 156 ± 8 to 174 ± 6 Ma and 152 ± 2 Ma for biotite grains extracted from metasedimentary and metamagmatic rocks of the same unit. Okay et al. (2014) also obtained 161 ± 3 to 169 ± 5 Ma ages for biotite grains from the metasedimentary rocks of the Geme Complex. In this present study, the measured isotopic ratios and calculated ages for muscovite grains from the metasedimentary rocks (schist, SV-3 and −6) are shown in Table S5. Individual muscovite grains from SV-3 sample yielded a weighted mean age of 285 ± 4 Ma (n = 12; Fig. 12a). Similarly, a weighted mean age of 281.0 ± 2.3 Ma is calculated here based on single muscovite crystals from sample SV-6 (n = 6; Fig. 12b, c).

5. Discussion

5.1. Geochemical nature of source areas

Immobile trace element characteristics (e.g., REEs and HFSEs) of the metasedimentary units studied here may provide significant information with regards to chemical composition and tectonic setting of the source area (e.g., Bhatia and Crook, 1986; Floyd and Leveridge, 1987; McLennan et al., 1993). The whole rock geochemical signatures of the metasedimentary rocks investigated here indicate that their protoliths were likely derived from source regions characterized by “acidic arc” and “felsic volcanic rocks” (Fig. 5a, b). On the basis of the Co/Th ratios, the samples from the Devrekani Massif and the Geme Complex may have been generated from more felsic magmatic rocks compared to those from the Serveçay Unit (Fig. 5b; McLennan et al., 1993). The relatively scattered distribution of Hf and La/Sc values for metasedimentary samples from the Devrekani Massif indicate that their source areas may be of a slightly different geochemical nature (Fig. 5a, b; Floyd and Leveridge, 1987; McLennan et al., 1993). The immobile elemental

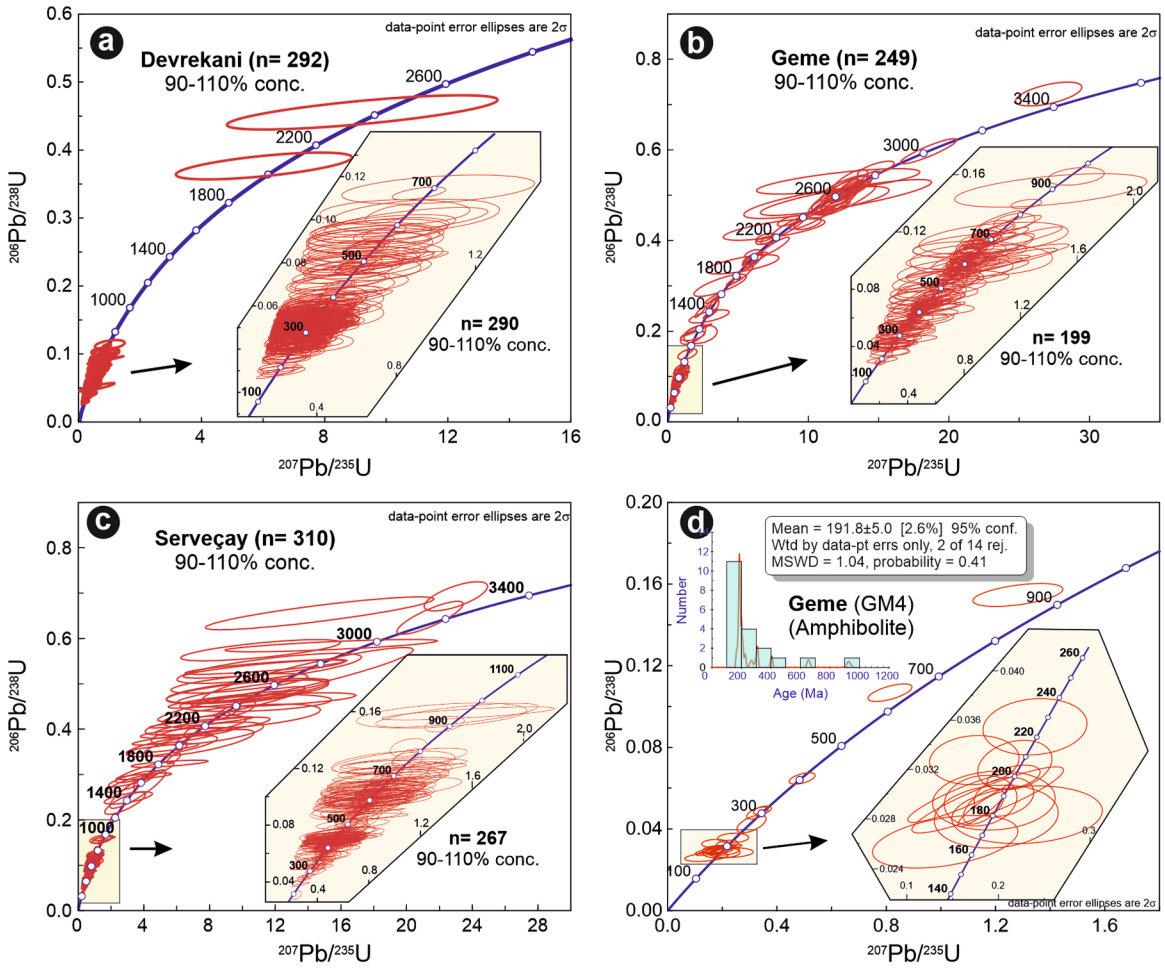

Fig. 6. $^{206}Pb/^{238}U$ vs $^{207}Pb/^{235}U$ concordia diagrams for zircon grains from metasedimentary rocks in **(a)** the Devrekani Massif, **(b)** the Geme Complex and **(c)** the Serveçay Unit. **(d)** $^{206}Pb/^{238}U$ vs $^{207}Pb/^{235}U$ concordia diagram for zircons from an amphibolite sample in the Geme Complex.

signatures for the samples reported here also reveal that these acidic source rocks may be continental arc in character from active margins (Fig. 5c, d; Bhatia and Crook, 1986). Lastly, the REEs patterns for the samples from all basement units show enrichments in LREEs over HREEs and these signatures support the presence of source areas that are of continental arc in nature (Fig. 5a). The negative Eu-anomalies recorded here may indicate that the protoliths of the samples were deposited in slightly oxic environments (e.g., Bau, 1991; Çimen et al., 2013). One sample from the Geme Complex that is characterized by a more depleted REE pattern may have been derived from a less felsic source area (Fig. 5a). The samples investigated here are characterized by geochemical features similar to those from upper crust (Rudnick and Gao, 2003) given their enrichments in Th, La and Ce coupled with negative Nb, Ta, P and Ti anomalies. Moreover, the presence of Th, La and Ce enrichments and Nb and Ta depletions could be further indicators for derivation from continental arc rocks (e.g., Pearce and Peate, 1995; Saccani, 2015).

5.2. Potential provenance regions

The metasedimentary rocks from the Devrekani Massif include mainly Carboniferous (48 %), Permian (19 %) and Devonian (11 %) zircon populations, and lesser amount of Neoproterozoic (7 %), Cambrian (5 %), Ordovician (3 %), Triassic (3 %), Silurian (2 %), Paleoproterozoic (1 %), and Early Jurassic (1 %) zircons (Fig. 7a). In contrast, the metasedimentary rocks from the Geme Complex are characterized by mainly Neoproterozoic (33 %) and Devonian (14 %) and lesser amount of Carboniferous (9 %), Archean (8 %), Paleoproterozoic (7 %), Silurian (7 %), Permian (5 %), Ordovician (5 %), Mesoproterozoic (5 %), Cambrian (4 %), Triassic (2 %) and Early Jurassic (1 %) zircon populations (Fig. 8a). Analogous to the Geme Complex, the metasedimentary rocks of the Serveçay Unit constitute mainly Neoproterozoic (37 %), Devonian (16 %), Silurian (11 %) and Ordovician (10 %) and lesser amount of Paleoproterozoic (7 %), Carboniferous (6 %), Cambrian (5 %), Archean (4 %), Mesoproterozoic (3 %) and Permian (2 %) zircon populations (Fig. 9a). The CL images of the youngest populations show oscillatory zoning and are thus consistent with a magmatic origin (Corfu et al., 2003).

With regards to potential source regions, the Devrekani Massif also contains well-defined Permo-Carboniferous orthogneisses that formed in a continental arc setting (316 ± 9 and 252 ± 9 Ma; Gücer et al., 2019). Apart from these magmatic rocks, the closest outcrop of Permo-Carboniferous granitoids is in the northern part of the Central Pontides (Fig. 1b and 2c; Sivrikaya, 298 ± 2 Ma, 300 ± 1 Ma and Deliktaş, 295 ± 1 Ma granitoids; next to the Serveçay Unit; Nzegge, 2008; Okay et al., 2014). Recent studies (Aysal et al., 2018; Babaoğlu et al., 2023) report the presence of middle Permian (*ca.* 253–261 Ma) magmatism in western IZT. Also, large slide-blocks of late Permian (260 ± 2 Ma) granitoids of IZT origin were described from the early Maastrichtian - middle Paleocene Taraklı Formation (Di Rosa et al., 2019) in the central Pontides. Therefore, these magmatic rocks may be the source regions of the dominant Carboniferous and Permian zircons in the metasedimentary rocks from the Devrekani Massif. It should be noted that other Permian and Carboniferous magmatic rocks have been reported in the Strandja

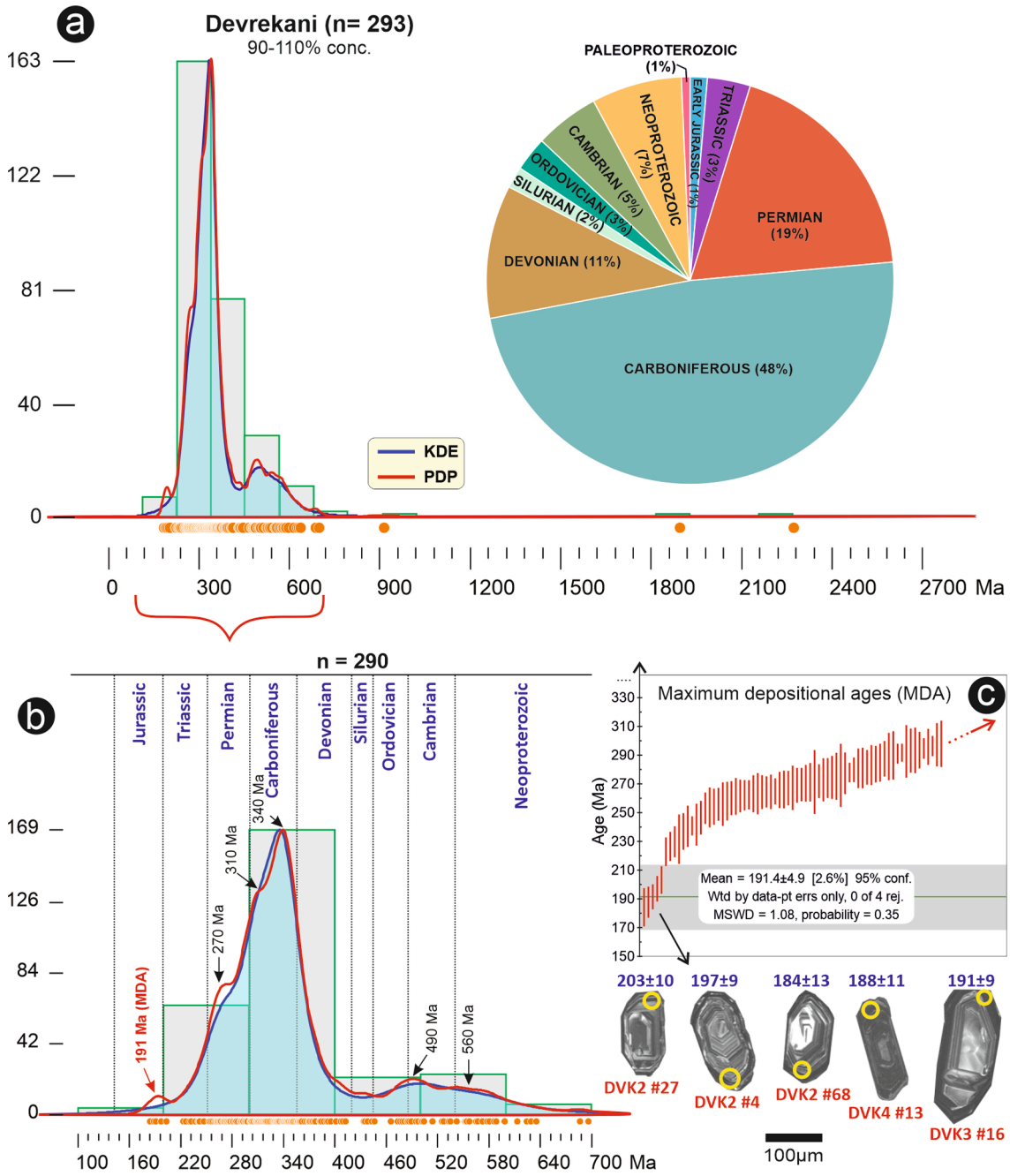

Fig. 7. **(a)** Kernel density estimation (KDE) plot comparing the curves of probability density (PDP) functions, and pie chart diagram showing the distribution of detrital zircon ages of the Devrekani Massif. **(b)** KDE diagram showing the detrital zircon age distribution from the Neoproterozoic era to the Jurassic period. **(c)** Maximum depositional age (MDA) diagram of the Devrekani Massif.

Massif (e.g., Üsküp and Kırklareli metagranites, *ca.* 257 and 309 Ma; Okay et al., 2001; Sunal et al., 2006), the SCT (e.g., Söğüt and Gümüşhane granitoids, *ca.* 327 and 324 Ma; Ustaömer et al., 2012; Topuz et al., 2010), and the Caucasus (e.g., *ca.* 317–331 Ma; Gamkrelidze et al., 2011) (Fig. 1a; for a detailed age compilation, see Okay and Topuz, 2017 and references therein).

The IZT includes various outcrops of Neoproterozoic metagranitoids (e.g., Karadere Unit and Bolu Massif, *ca.* 590–560 Ma, Chen et al., 2002; Ustaömer et al., 2005; Okay et al., 2008), and these areas could be potential source areas of the Neoproterozoic zircons (<~600 Ma) reported from the metasedimentary rocks from both the Geme Complex and the Serveçay Unit (Fig. 1a). The other dominant population in the samples from the Geme Complex and the Serveçay Unit is represented by Devonian zircons, and the potential source region of these zircons may be Devonian granitoids (e.g., Karacabey, Çamlık and Bayatlar granitoids, *ca.* 389 to 401 Ma; Okay et al., 1996; Aysal et al., 2012a, b; Sunal, 2012) outcropping in the western SCT (Fig. 1a). The closest outcrop of Silurian magmatism has been reported in the western SCT (Sarıcakaya Massif, *ca.* 445 to 425 Ma; Topuz et al., 2020), and this region represents the potential source area of the Silurian zircons in both the Geme Complex and the Serveçay Unit. Moreover, the association of Silurian and Early Devonian magmatic rocks has been recently reported in another region located in the western SCT (Bozüyük and Borçak metagranitoids, *ca.* 431 to 403 Ma; Karslı et al., 2020). If these recent findings are supported by further evidence, it would indicate that SCT, Geme and Serveçay were paleogeographically closely related. The Ordovician

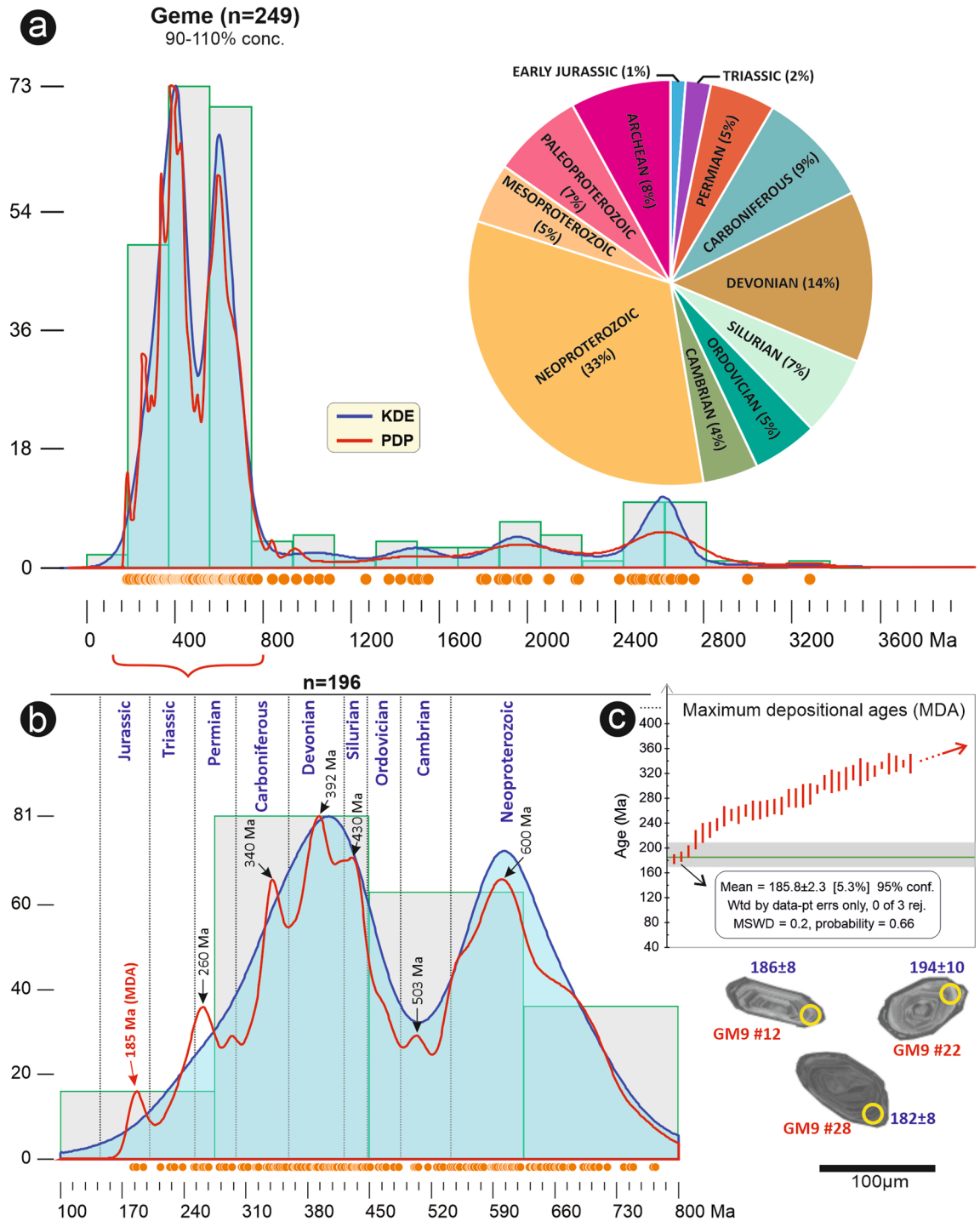

Fig. 8. **(a)** Kernel density estimation (KDE) plot comparing the curves of probability density (PDP) functions, and pie chart diagram showing the distribution of detrital zircon ages of the Geme Complex. **(b)** KDE diagram showing the detrital zircon age distribution from the Neoproterozoic era to the Jurassic period. **(c)** Maximum depositional age (MDA) diagram of the Geme Complex.

zircon populations in both the Geme Complex and the Serveçay Unit could have been derived from arc-related Ordovician magmatics reported from the IZT (Pamukova-Armutlu regions and Bolu massif, *ca.* 484 to 443 Ma; Şen, 2023), or the western TAP (Kapanca metagranitoid, *ca.* 467 Ma, Okay et al., 2008; Sarıkaya metagranite, *ca.* 446 Ma, Özbey et al., 2013). Recently, the occurrence of early Cambrian plutons has been reported by Yılmaz et al. (2022) in the Strandja Massif (Binkılıç and İhsaniye plutons, *ca.* 525 to 548 Ma), and these magmatic rocks may be a potential source region for the minor Cambrian zircon populations reported here.

Limited outcrops of bimodal Permo-Triassic magmatic rocks of continental crust origin are described from the Moesian and Scythian platforms as well as the Variscan belt in Europe (Nikishin et al., 2002; Seghedi, 2011; Chang et al., 2020; Yuan et al., 2020; Ondrejka et al., 2021; Huang et al., 2022). However, the Triassic subduction accretion complexes, namely the Karakaya Complex of the SCT (Ustaömer et al., 2016) and the Küre Complex of the Central Pontides (Fig. 1b; Karslıoğlu et al., 2012), contain significant amounts of Triassic detrital zircons, and these units may represent the source areas of the recycled Triassic zircons investigated here. The closest Early to Middle Jurassic outcrop of

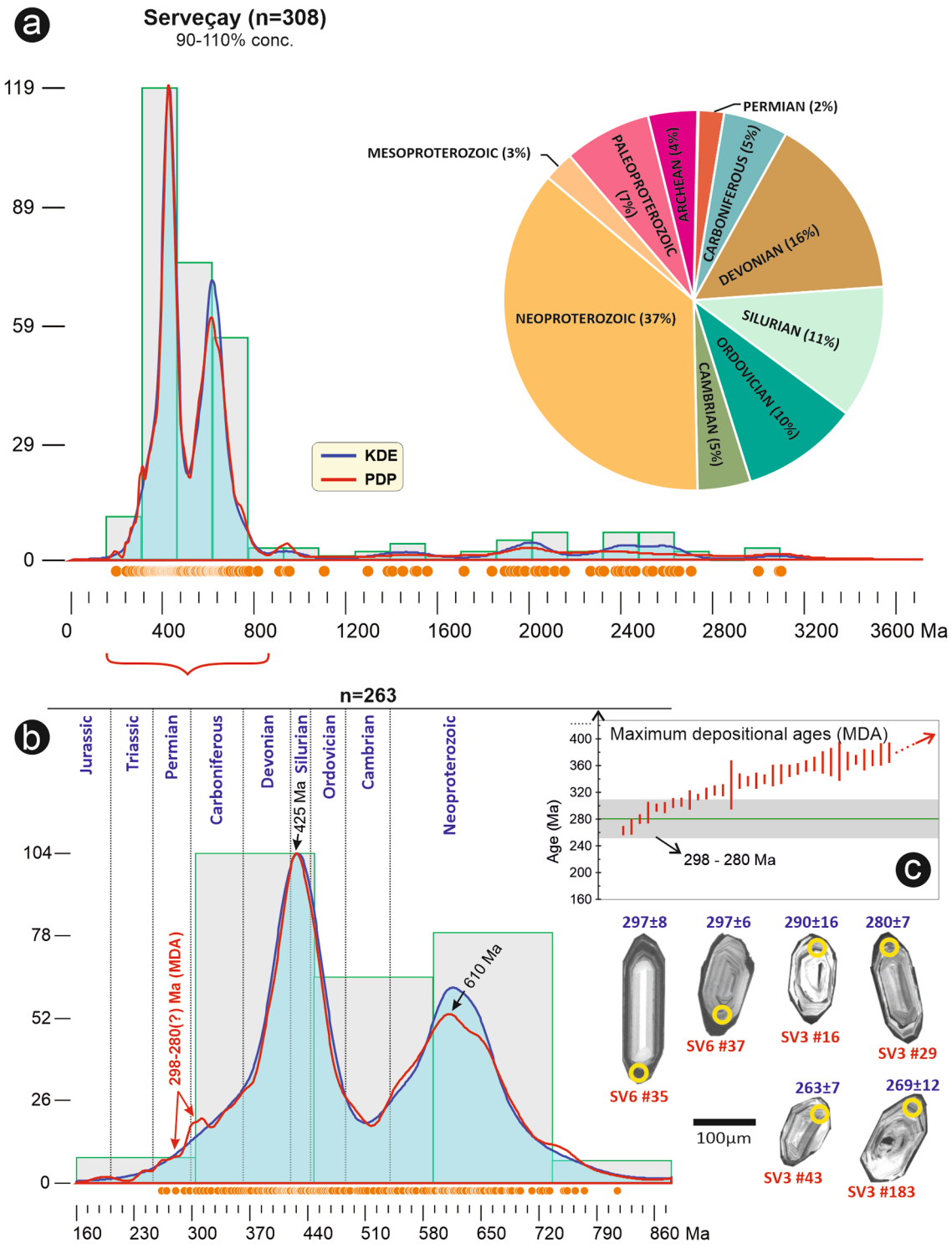

Fig. 9. **(a)** Kernel density estimation (KDE) plot comparing the curves of probability density (PDP) functions, and pie chart diagram showing the distribution of detrital zircon ages of the Serveçay Unit. **(b)** KDE diagram showing the detrital zircon age distribution from the Neoproterozoic era to the Jurassic period. **(c)** Maximum depositional age (MDA) diagram of the Serveçay Unit.

magmatic rocks is located in the southern of the Central Pontides and the western SCT (Mudurnu formation, Genç and Tüysüz, 2010). The presence of other Early Jurassic magmatic rocks is known in the eastern SCT (Olur region and the Demirkent Intrusive Complex, *ca.* 184 and 185 Ma; Dokuz et al., 2006; Dokuz and Sünnetçi, 2019). The Early Jurassic zircons from both the Devrekani Massif and the Geme Complex may have been sourced from these regions. The minor populations of Mesoproterozoic zircons in the Geme Complex and the Serveçay Unit could have been recycled from the metasedimentary rocks in the Karadere Unit (eastern IZT), which is characterized predominantly by Mesoproterozoic-age zircons (Göncüoğlu et al., 2022).

Outcrops of igneous Archean- and Paleoproterozoic-aged rocks have yet to be reported within the Central Pontides and the proximal, surrounding areas. The potential source region of Archean and Paleoproterozoic zircons reported from both the Geme Complex and the Serveçay Unit may be the Archean-Paleoproterozoic Ukrainian Shield

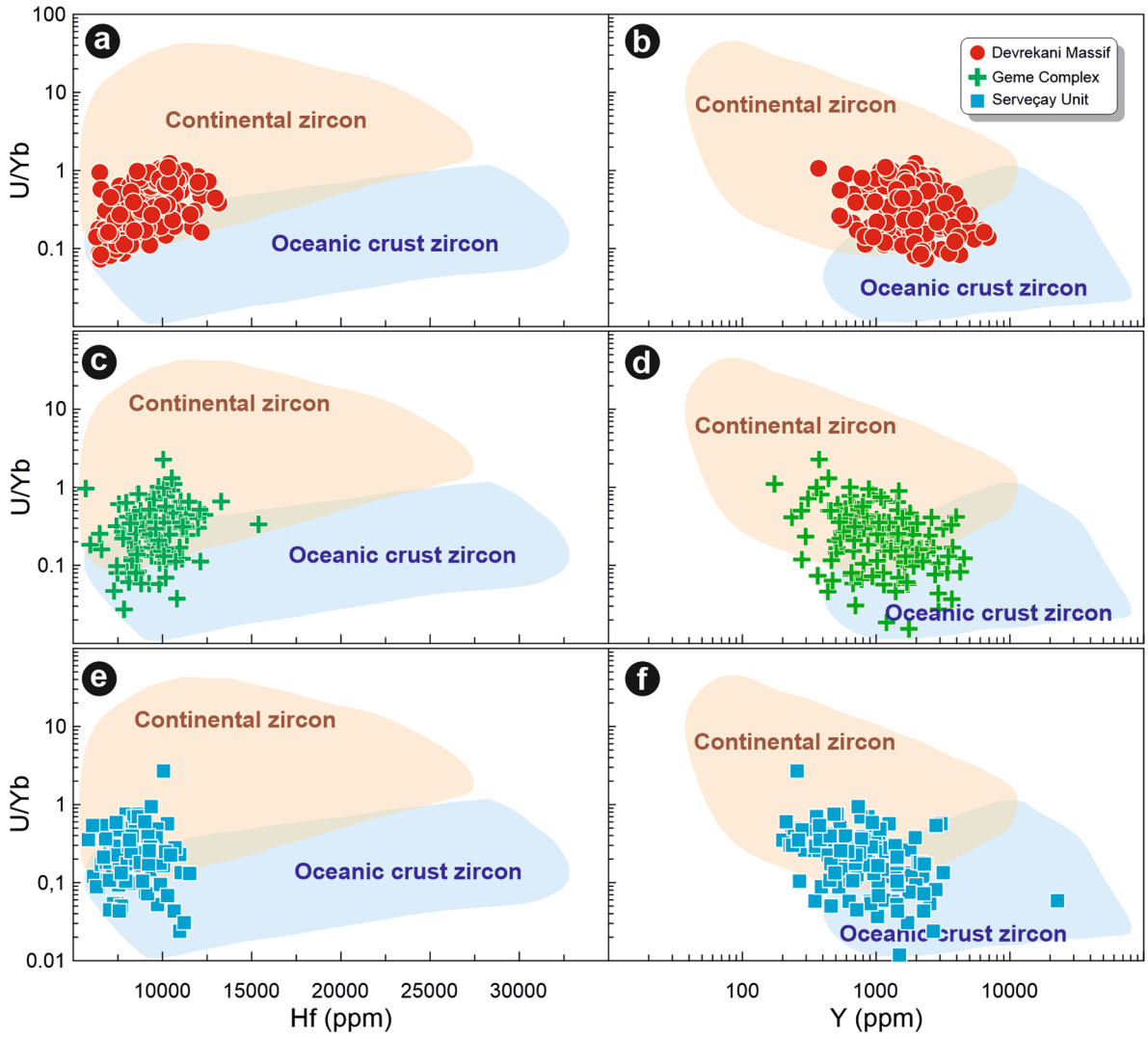

Fig. 10. U/Yb vs Hf and Y discrimination diagrams for zircons from the metasedimentary rocks in **(a-b)** the Devrekani Massif, **(c-d)** the Geme Complex, **(e-f)** the Serveçay Unit.

(Claesson et al., 2015) to the north (Fig. 1a); similar aged zircon populations have also been reported from the Lower and Upper Cretaceous turbidites in the Central Pontides (Okay et al., 2013; Akdoğan et al., 2017, 2019). Of note, there is no extensive source area for the 610–600 Ma age peaks for zircons (n = 133; 820 to 579 Ma) from both the Geme Complex and the Serveçay Unit (Fig. 8a and 9b). Therefore, Hf isotope analyses were conducted for these zircon populations to better understand the nature of their source region. The Hf isotope data indicate derivation from mainly crustal sources but do also exhibit some mantle signatures (Fig. 11a, b). Recently, Göncüoğlu et al. (2022) reported an age of 603 ± 2 Ma for a single orthogneiss sample from the Karadere Unit (eastern IZT); however, more extensive source regions are required to generate these distinct age peaks and thus further geochronological studies are needed to help identify potential source regions.

5.3. Maximum depositional ages and metamorphism histories

It is well-documented that the Central Pontides are composed of geological units of IZT in the west and the remnants of the IPSZ in the south (Fig. 1a, e.g., Göncüoğlu et al., 2012; Okay and Topuz, 2017; Çimen et al., 2018). However, and of note, the pre-Jurassic paleogeographic setting and the geological evolution of the units in the northern Central Pontides is still poorly understood. The pre-Jurassic lithological assemblages of this area comprise the Triassic Küre Complex, the late Paleozoic granitoids and the Devrekani Massif, the Geme Complex, and the Serveçay Unit (Fig. 1b). Here, it has been assumed thus far that the Devrekani Massif, the Geme Complex, and the Serveçay Unit represent the pre-Cambrian or Paleozoic basement units of the Central Pontides (Tüysüz, 1990; Aydın et al., 1995; Boztuğ et al., 1995; Kozur et al., 2000; Nzegge, 2008; Okay and Nikishin, 2015; Gücer et al., 2019; Çimen, 2020a).

The detrital zircon age populations reported here (the youngest zircon age, 184 ± 13 Ma and the youngest peak age, n = 5, 1 %, 191.0 ± 4.9 Ma; Dickinson and Gehrels, 2009), however, indicate that the protoliths of metasedimentary rocks from the Devrekani Massif could have been deposited until the Early Jurassic period (Fig. 7b). Similarly, the youngest zircon age (182 ± 8 Ma) and the youngest peak age (n = 3, 185.0 ± 2.3 Ma; Dickinson and Gehrels, 2009) from the metasedimentary rocks from the Geme Complex clearly indicate that this unit may have been deposited in the Early Jurassic as well (Fig. 8b). Of note, the youngest zircons show subhedral to rounded forms associated with oscillatory zoning and fracturing, which is consistent with a magmatic origin. Moreover, an amphibolite sample taken from the Geme Complex has been dated as Early Jurassic (191 ± 5 Ma; Fig. 6d) in this study and this finding also supports the Early Jurassic age for the Geme Complex.

Aydın et al. (1995) considered the Serveçay Unit as a part of Triassic

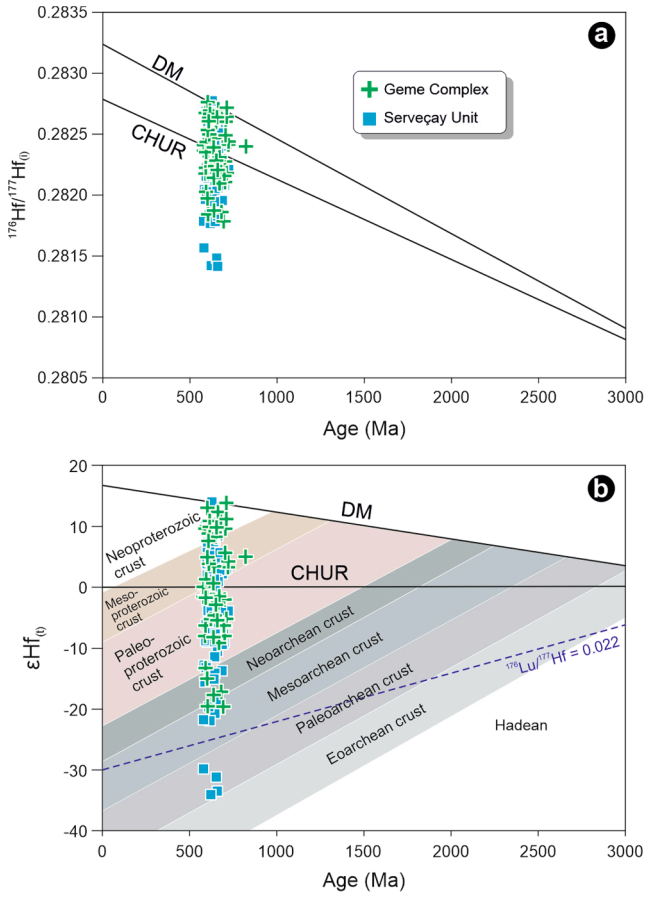

Fig. 11. (a) $^{176}Hf/^{177}Hf$ and (b) εHf(t) vs Age diagrams for zircons (820 to 582 Ma) from the metasedimentary rocks in the Geme Complex and the Serveçay Unit (diagram modified after Kostrovitsky et al., 2016; Dana et al., 2023).

Küre Complex, whereas Kozur et al. (2000) suggested that this unit is another member of Paleozoic Variscan basement that occur within the SCT (Fig. 1a). Okay et al. (2015) also proposed that the Serveçay Unit is of Paleozoic age since it is cut by Permo-Carboniferous granitoids (*ca.* 305 to 290 Ma). The youngest peak age (n = 8, *ca.* 298 to 280 Ma; Dickinson and Gehrels, 2009) from the metasedimentary units in the Serveçay Unit indicate that this unit may have been deposited during the early Permian (Fig. 9b), and may indeed represent a Variscan basement in the Central Pontides. Contrarily, based on the maximum depositional age obtained in this study, the contact between the Serveçay Unit and the Permo-Carboniferous granitoids should be considered tectonic in nature instead of an intrusive one.

Regarding the timing of metamorphism of the studied units, a Middle Jurassic metamorphism age has been well-documented for the Devrekani Massif (K-Ar method, 170 ± 10 to 149 ± 4 Ma, Yılmaz and Bonhomme, 1991; Ar-Ar method, 151 ± 1 to 146 ± 2 Ma, Okay et al., 2014; Ar-Ar method, 163 ± 5 to 152 ± 5 Ma, Gücer et al., 2016). In addition, Okay et al. (2014) reported a Middle Jurassic (169 ± 5 to 161 ± 3 Ma) metamorphism age for the Geme Complex. In contrast, a Carboniferous age (K-Ar method, 311.0 ± 6.2 Ma, Aydın et al., 1995) has been previously reported for the Serveçay Unit. However, the new and more precise Ar-Ar data reported here suggests a Permian metamorphism age for this unit (Fig. 12). Overall, the ages presented here indicate that the Devrekani and the Geme Complex were metamorphosed during the Middle Jurassic, whereas the Serveçay Unit incurred metamorphism in the late early Permian.

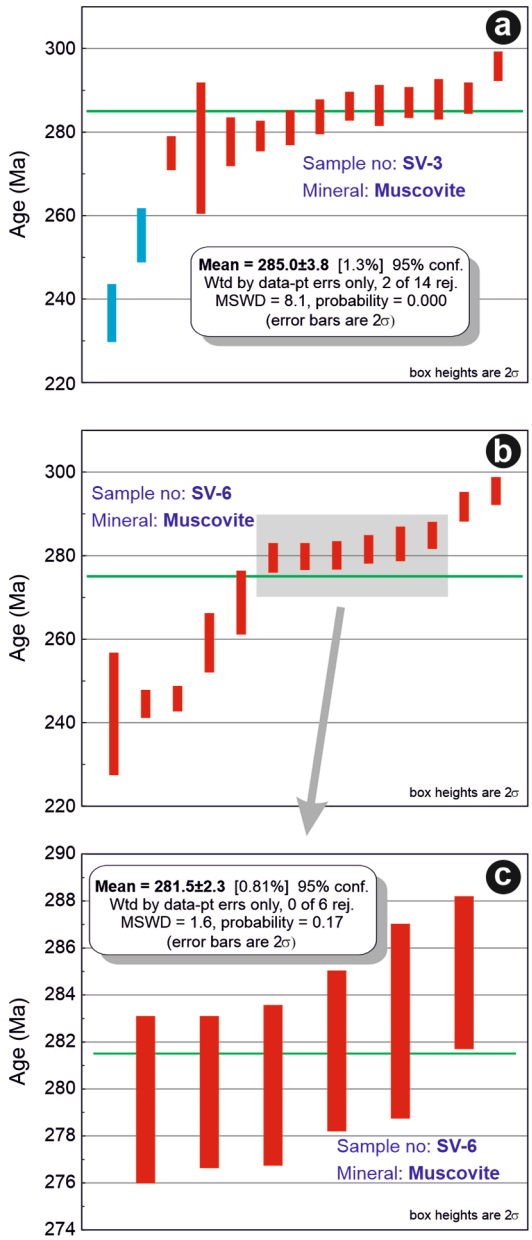

Fig. 12. ^{40}Ar-^{39}Ar weighted mean ages for muscovite grains from **(a)** SV-3 and **(b-c)** SV-6 metasedimentary samples in the Serveçay Unit.

5.4. *Tectonic implications*

The combined detrital zircon trace element geochemistry, U-Pb geochronology, and Ar-Ar metamorphism ages reported in this study suggest the presence of different tectonic evolution paths for the Devrekani Massif, the Geme Complex, and the Serveçay Unit (Table 3).

The Serveçay Unit is mainly characterized by Neoproterozoic and Devonian zircons (53 %) and has a Permian maximum depositional and age of metamorphism (Fig. 9, Table 3). Therefore, it may have been deposited in an area close to the margins of IZT and western SCT since this continental fragment includes potential Neoproterozoic and Devonian magmatic source areas (e.g., Okay et al., 1996; Chen et al., 2002; Ustaömer et al., 2005; Sunal, 2012). Subsequently, the Serveçay Unit could have been metamorphosed during the Permian period in relation to the Variscan events that is obviously traced throughout the SCT (Fig. 1a, e.g., Okay and Topuz, 2017).

Similar to the Serveçay Unit, the Geme Complex constitutes mostly Neoproterozoic and Devonian zircons (47 %). However, it has a distinct

Table 3
Comparison of the data obtained from the Devrekani Massif, the Geme Complex and the Serveçay Unit.

Unit	Devrekani Massif	Geme Complex	Serveçay Unit
Petrography	Paragneiss	Paragneiss, Amphibolite	Phyllite, Micaschist
Provenance signatures	Clastics derived from an active continental margin, where mostly Permo-Carboniferous, less Devonian felsic igneous rocks are common.	Clastics derived from an active continental margin, where mostly Neoproterozoic, less Devonian and Permo-Carboniferous aged felsic igneous rocks are common.	Clastics derived from an active continental margin, where mostly Neoproterozoic, less Devonian, Silurian and Ordovician felsic igneous rocks are common.
Maximum depositional age (MDA)	*ca.* 191 Ma (early Jurassic)	*ca.* 185 Ma (early Jurassic)	*ca.* 298–280 Ma (Permian)
$^{40}Ar/^{39}Ar$ age	*ca.* 174–156 Ma (Okay et al., 2014; Gücer et al., 2016, 2019)	*ca.* 172–164 Ma (Okay et al., 2014)	*ca.* 285–281 Ma (this study)
Detrital zircon U-Pb geochronology	*ca.* 2271 – 184 Ma (Paleoproterozoic – early Jurassic)	*ca.* 3279 – 182 Ma (Archean - early Jurassic)	*ca.* 3098 – 280 Ma (Archean - early Jurassic)
Th/U raitos	0.02–0.1 (n = 17) 0.11–1.74 (n = 276)	0.01–0.1 (n = 24) 0.11–2.29 (n = 229)	0.01–0.1 (n = 18) 0.11–2.49 (n = 296)
Lu-Hf isotopes from zircon minerals	not analyzed	For Neoproterozoic (820–579 Ma, n = 55) zircons; $^{176}Hf/^{177}Hf_{(i)}$: 0.281788—0.282769 $\varepsilon Hf_{(t)}$: (-19.59) - (+13.94)	For Neoproterozoic (721–579 Ma, n = 78) zircons; $^{176}Hf/^{177}Hf_{(i)}$: 0.281417—0.282780 $\varepsilon Hf_{(t)}$: (-34.06) - (+14.12)

Early Jurassic maximum depositional age and was metamorphosed during the Middle Jurassic (Figs. 8 and 13; Table 3). Here, the dominant zircon populations are Neoproterozoic and Devonian in age, and may indicate that the Geme Complex may have been deposited in an area proximal to the Serveçay Unit; in addition, they both could have been sourced from similar magmatic units outcropping in the IZT and the western SCT. However, the deposition in the Geme Complex may have lasted until the Early Jurassic period in a marginal basin related to the Intra-Pontide Ocean (e.g., Robertson and Ustaömer, 2004; Göncüoğlu et al., 2012; Çimen et al., 2016, 2017, 2018; Ellero et al., 2015, 2021; Frassi et al., 2018, 2020). Subsequent to its deposition, the Geme Complex could have been emplaced on the active margin of the SCT and metamorphosed during the Middle Jurassic.

In contrast to the Serveçay Unit and the Geme Complex, the Carboniferous- and Permian-aged zircons make up 67 % of total detrital zircon population for the Devrekani Massif (Fig. 7 and Table 3). Although it has a similar Early Jurassic maximum deposition and Middle Jurassic age for metamorphism as with the Geme Complex, its distinct detrital zircon population distribution indicates that the protoliths of the Devrekani metasediments may have been deposited in a different basin

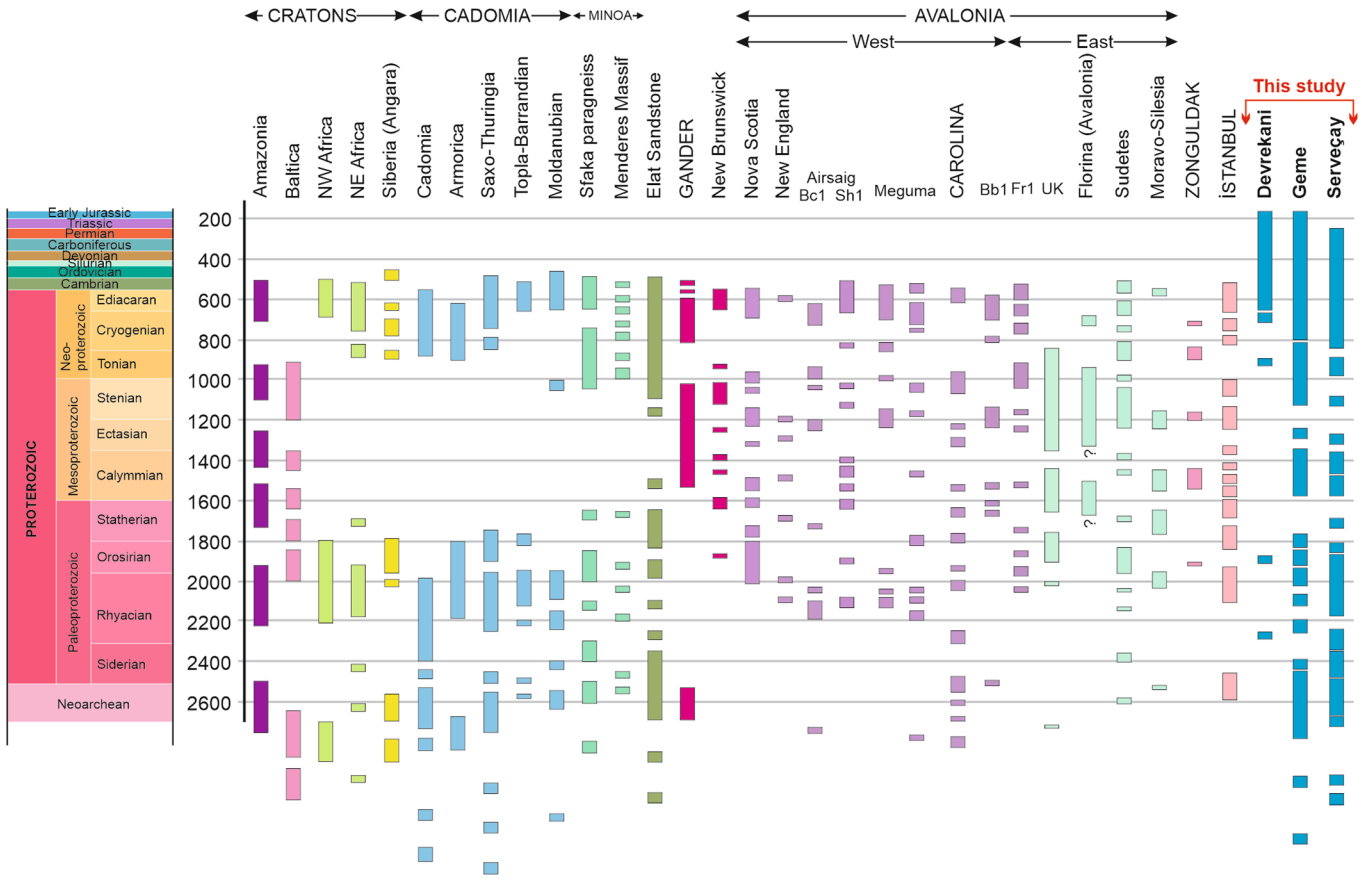

Fig. 13. Distribution of detrital zircon ages and/or igneous events encountered in major cratons and many *peri*-Gondwanan terranes (modified from Ustaömer et al., 2011 and references therein).

than the Geme Complex. These clastic rocks may have been mainly sourced from the Permo-Carboniferous igneous rocks reported in the basement of the Devrekani Massif (Gücer et al., 2019) in the north of the Central Pontides during the Early Jurassic (Nzegge, 2008; Okay et al., 2015). Similar to the Geme Complex, after its emplacement within the SCT, it could have been metamorphosed during the Middle Jurassic and attributed to the tectonic evolution of Intra-Pontide Ocean (e.g. Marroni et al., 2020).

Furthermore, the trace element characteristics (U/Yb vs. Hf) of zircons from the metasedimentary units in the Devrekani Massif indicate that they were most likely derived from a source region consisting of continental crust (Fig. 10a, b; Grimes et al., 2007). However, the zircons from the metasedimentary units in the Geme Complex and the Serveçay Unit may have been derived from both continental and oceanic crusts (Fig. 10c, d, e, f; Grimes et al., 2007). Hence, these pronounced differences in geochemical signatures also support our hypothesis that the metasedimentary units in the Devrekani Massif were deposited in a different basin with a relatively different hinterland compared to that for the Geme Complex and the Serveçay Unit.

6. Conclusions

The combined whole rock geochemistry, detrital zircon U-Pb ages and corresponding trace element signatures, and mica Ar-Ar age data reported here provide constraints for understanding the provenances, depositional ages, and tectonic evolution of the Devrekani Massif, the Geme Complex, and the Serveçay Unit in the basement of the Central Pontides, and these are listed below:

- The whole rock geochemical signatures of the metasedimentary rocks indicate derivation from arc-related felsic magmatic rocks within an active continental margin.
- The protoliths for the metasedimentary rocks in the Devrekani Massif were mainly sourced from the proximal Permo-Carboniferous magmatic rocks outcropping in the Central Pontides. In contrast, the protoliths for the metasedimentary rocks in the Geme Complex and the Serveçay Unit were mostly derived from the Neoproterozoic and Devonian magmatics located in the IZT and the western SCT. These findings clearly indicate that the Devrekani Massif may have been paleogeographically located in a different position relative to the Geme Complex and the Serveçay Unit.
- Depleted mantle εHf model ages for zircons from the Geme Complex and the Serveçay Unit range from 820 to 579 Ma (610–600 Ma peak ages), which suggests that the dominant signature is a crustal source, but zircons of mantle origin are also present.
- The Devrekani Massif and the Geme Complex were deposited and metamorphosed during the Early Jurassic and Middle Jurassic periods, respectively, but the Serveçay Unit was deposited and metamorphosed in the Permian. Consequently, the Devrekani Massif and the Geme Complex were most likely in a similar position during the Jurassic accretion events within the Intra-Pontide Ocean. In contrast, the Serveçay Unit was solely involved in the late Paleozoic deformation and metamorphism event attributed to the closure of a Variscan marginal basin.

CRediT authorship contribution statement

Okay Çimen: Project administration, Methodology, Investigation, Data curation, Conceptualization, Software, Visualization, Writing – original draft, Writing – review & editing. **Mehmet Ali Gücer:** Supervision, Writing – review & editing. **Cüneyt Akal:** Methodology, Software, Visualization, Writing – review & editing. **Mehmet Cemal Göncüoğlu:** Supervision, Writing – review & editing. **Mehmet Arslan:** Supervision, Writing – review & editing. **Antonio Simonetti:** Data curation, Methodology, Software, Writing – review & editing. **Fatih Karaoğlan:** Data curation, Methodology, Software, Writing – review & editing.

Declaration of competing interest

The authors declare that they have no known competing financial interests or personal relationships that could have appeared to influence the work reported in this paper.

Data availability

Data will be made available on request.

Acknowledgements

This paper is dedicated to the memory of Prof. Dr. Aral Okay, who passed away recently. We would not be able to figure out the geological problems of the Central Pontides without his valuable contributions. This study was financially supported by TÜBİTAK (Scientific and Technological Research Council of Türkiye) with project number 118Y507. We appreciate the comments provided by two anonymous reviewers, which have resulted in an improved manuscript. Also, we would like to thank Dr. Ibrahim Uysal (Associate Editor) for handling our manuscript.

Appendix A. Supplementary data

Supplementary data to this article can be found online at https://doi.org/10.1016/j.jseaes.2024.106134.

References

Akdoğan, R., Okay, A.I., Sunal, G., Tari, G., Meinhold, G., Kylander-Clark, A.R.C., 2017. Provenance of a large lower cretaceous turbidite submarine fan complex on the active laurasian margin: central pontides, northern Turkey. J. Asian Earth Sci. 134, 309–329.

Akdoğan, R., Okay, A.I., Dunkl, I., 2019. Striking Variation in the provenance of the lower and upper cretaceous turbidites in the central pontides (northern Turkey) related to the opening of the Black Sea. Tectonics 38 (3), 1050–1069.

Armstrong-Altrin, J.S., Lee, Y.I., Verma, S.P., Ramasamy, S., 2004. Geochemistry of sandstones from the Upper Miocene kudankulam formation, southern India: implications for provenance, weathering, and tectonic setting. J. Sediment. Res. 74 (2), 285–297.

Aydın, M., Demir, O., Özçelik, Y., Terzioğlu, N., Satır, M., 1995. A geological revision of İnebolu, Devrekani, Ağlı and Küre areas: new observations in Paleo-Tethys - Neo-Tethys sedimentary successions. In: Geology of the Black Sea region. General Directorate of Mineral Research Exploration and Chamber of Geological Engineers, Ankara, Turkey.

Aygül, M., Okay, A.I., Oberhänsli, R., Sudo, M., 2016. Pre-collisional accretionary growth of the southern laurasian active margin, central pontides, Turkey. Tectonophysics 671, 218–234.

Aysal, N., Öngen, S., Peytcheva, I., Keskin, M., 2012a. Origin and evolution of the Havran unit, Western Sakarya basement (NW Turkey): new LA-ICP-MS U-pb dating of the metasedimentary-metagranitic rocks and possible affiliation to avalonian microcontinent. Geodin. Acta 25 (3–4), 226–247.

Aysal, N., Ustaömer, T., Öngen, S., Keskin, M., Köksal, S., Peytcheva, I., Fanning, M., 2012b. Origin of the Early-middle devonian magmatism in the Sakarya zone, NW Turkey: geochronology, geochemistry and isotope systematics. J. Asian Earth Sci. 45, 201–222.

Aysal, N., Yılmaz Şahin, S., Güngör, Y., Peytcheva, I., Öngen, S., 2018. Middle Permian–early triassic magmatism in the Western pontides, NW Turkey: geodynamic significance for the evolution of the paleo-tethys. J. Asian Earth Sci. 164, 83–103.

Babaoğlu, C., Topuz, G., Okay, A.I., Köksal, S., Wang, J.-M., Toksoy-Köksal, F., 2023. Middle permian basic and acidic volcanism in the Istanbul zone (NW Turkey): evidence for post-variscan extensional magmatism. Int. Geol. Rev. 65 (21), 3435–3452.

Bau, M., 1991. Rare-earth element mobility during hydrothermal and metamorphic fluid-rock interaction and the significance of the oxidation state of europium. Chem. Geol. 93 (3–4), 219–230.

Bhatia, M.R., Crook, K.A.W., 1986. Trace element characteristics of graywackes and tectonic setting discrimination of sedimentary basins. Contrib. Miner. Petrol. 92 (2), 181–193.

Boynton, W.V., 1984. Cosmochemistry of the Rare Earth elements: meteorite studies. In: Henderson, P. (Ed.), Developments in Geochemistry. Elsevier, pp. 63–114.

Boztuğ, D., Yılmaz, O., 1995. Metamorphism and geological evolution of the daday-devrekani massif, Kastamonu region, Western pontides, Northern Turkey. Geological Bulletin of Turkey 38 (1), 33–52 in Turkish with English abstract.

Boztuğ, D., Debon, F., Le Fort, P., Yılmaz, O., 1995. High compositional diversity of the middle jurassic Kastamonu Plutonic Belt, northern Anatolia, Turkey. Turk. J. Earth Sci. 4, 67–86.
Çelik, Ö.F., Marzoli, A., Marschik, R., Chiaradia, M., Neubauer, F., Öz, İ., 2011. Early-middle jurassic intra-oceanic subduction in the İzmir-Ankara-Erzincan Ocean, Northern Turkey. Tectonophysics 509 (1–2), 120–134.
Chang, R., Neubauer, F., Liu, Y., Genser, J., Jin, W., Yuan, S., Guan, Q., Huang, Q., Li, W., 2020. Subduction of a rifted passive continental margin: the pohorje case of eastern Alps–constraints from geochronology and geochemistry. Swiss J. Geosci. 113 (1), 14.
Chen, F., Siebel, W., Satir, M., Terzioğlu, M., Saka, K., 2002. Geochronology of the Karadere basement (NW Turkey) and implications for the geological evolution of the Istanbul zone. Int. J. Earth Sci. 91 (3), 469–481.
Çimen, O., 2020a. Geochemical characteristics of a pre-middle jurassic oceanic crust fragment from the central pontides in northern Turkey: geodynamic implications on intra-oceanic subduction initiation. Geochemistry 80 (1), 125535.
Çimen, O., 2020b. Geochemical characteristics of the adakite-like dodurga pluton (central pontides, N Turkey): implications for middle triassic continental arc magmatism in southern Black Sea region. Int. J. Earth Sci. 109 (3), 809–829.
Çimen, O., Koç, Ş., Sarı, A., 2013. Rare Earth element (REE) geochemistry and genesis of oil shales around Dağhacilar Village, Göynük-Bolu, Turkey. Oil Shale 30 (3), 419–440.
Çimen, O., Göncüoğlu, M.C., Sayit, K., 2016. Geochemistry of the metavolcanic rocks from the çangaldağ complex in the central pontides: implications for the middle jurassic arc-back-arc system in the neotethyan intra-Pontide Ocean. Turk. J. Earth Sci. 25 (6), 491–512.
Çimen, O., Göncüoğlu, M.C., Simonetti, A., Sayit, K., 2017. Whole rock geochemistry, zircon U-pb and hf isotope systematics of the çangaldağ pluton: evidences for middle jurassic continental arc magmatism in the central pontides, Turkey. Lithos 290–291, 136–155.
Çimen, O., Göncüoğlu, M.C., Simonetti, A., Sayit, K., 2018. New zircon U-pb LA-ICP-MS ages and hf isotope data from the central pontides (Turkey): geological and geodynamic constraints. J. Geodyn. 116, 23–36.
Claesson, S., Bibikova, E., Shumlyanskyy, L., Dhuime, B., Hawkesworth, C.J., 2015. The oldest crust in the ukrainian shield – Eoarchaean U-pb ages and Hf–Nd constraints from enderbites and metasediments. Geol. Soc. Lond. Spec. Publ. 389, 227–259.
Corfu, F., Hanchar, J.M., Hoskin, P.W.O., Kinny, P., 2003. Atlas of Zircon Textures, in: Finch, R., J., Hanchar, J., M. (Eds.), Zircon. Reviews in Mineralogy and Geochemistry, pp. 469-500.
Cullers, R.L., 1995. The controls on the major- and trace-element evolution of shales, siltstones and sandstones of Ordovician to tertiary age in the Wet Mountains region, Colorado, U.S.A. Chemical Geology 123(1–4), 107–131.
Dana, C.D.P., Agangi, A., Idrus, A., Chelle-Michou, C., Lai, C.-K., Ishida, M., Guillong, M., González-Álvarez, I., Takahashi, R., Yano, M., Mimura, K., Ohta, J., Kato, Y., Simbolon, D.R., Xia, X.-P., 2023. The Age and Origin of the Ruwai Polymetallic Skarn Deposit, Indonesia: Evidence of Cretaceous Mineralization in the Central Borneo Metallogenic Belt. Economic Geology.
Di Rosa, M., Farina, F., Marroni, M., Pandolfi, L., Göncüoğlu, M.C., Ellero, A., Ottria, G., 2019. U-pb zircon geochronology of intrusive rocks from an exotic block in the late cretaceous – paleocene Taraklı flysch (northern Turkey): constraints on the tectonics of the intrapontide suture zone. J. Asian Earth Sci. 171, 277–288.
Dickinson, W.R., Gehrels, G.E., 2009. Use of U-pb ages of detrital zircons to infer maximum depositional ages of strata: a test against a Colorado plateau mesozoic database. Earth Planet. Sci. Lett. 288 (1–2), 115–125.
Dokuz, A., Sünnetçi, K., 2019. Jurassic acidic magmatism in a back-arc setting, eastern Sakarya zone, Turkey: geochemical constraints and an evolutionary model. Lithos 332–333, 312–327.
Dokuz, A., Tanyolu, E., Genç, S., 2006. A mantle- and a lower crust-derived bimodal suite in the yusufeli (Artvin) area, NE Turkey: trace element and REE evidence for subduction-related rift origin of Early jurassic demirkent intrusive complex. Int. J. Earth Sci. 95 (3), 370–394.
Ellero, A., Ottria, G., Sayit, K., Catanzariti, R., Frassi, C., Göncüoğlu, M.C., Marroni, M., Pandolfi, L., 2015. Geological and geochemical evidences for a late cretaceous continental arc in the central pontides, Northern Turkey. Ofioliti 40 (2), 73–90.
Ellero, A., Frassi, C., Göncüoğlu, M.C., Lezzerini, M., Marroni, M., Ottria, G., Pandolfi, L., Sayit, K., Tamponi, M., 2021. Geological, structural and mineralogical approach to investigate the evolution of low- and very low-grade metamorphic units from the intra-pontide suture zone, central pontides, Turkey. J. Earth Sci. 32, 1512–1527.
Floyd, P.A., Leveridge, B.E., 1987. Tectonic environment of the devonian gramscatho basin, south Cornwall: framework mode and geochemical evidence from turbiditic sandstones. J. Geol. Soc. London 144 (4), 531–542.
Floyd, P.A., Göncüoğlu, M.C., Winchester, J.A., Yaliniz, M.K., 2000. Geochemical Character and tectonic environment of neotethyan ophiolitic fragments and metabasites in the central anatolian crystalline complex, Turkey. Geol. Soc. Lond. Spec. Publ. 173 (1), 183–202.
Floyd, P.A., Winchester, J.A., 1978. Identification and discrimination of altered and metamorphosed volcanic rocks using immobile elements. Chem. Geol. 21 (3–4), 291–306.
Frassi, C., Marroni, M., Pandolfi, L., Göncüoğlu, M.C., Ellero, A., Ottria, G., Sayit, K., McDonald, C.S., Balestrieri, M.L., Malasoma, A., 2018. Burial and exhumation history of the daday unit (central pontides, Turkey): implications for the closure of the intra-pontide oceanic basin. Geol. Mag. 155 (2), 356–376.
Frassi, C., Rebay, G., Marroni, M., Sayit, K., Göncüoğlu, M.C., Ellero, A., Ottria, G., Pandolfi, L., 2020. Metamorphic imprint of ridge subduction on the neo-tethyan ophiolites from the saka unit (central pontides, northern Turkey). J. Asian Earth Sci. 200, 104468.
Gamkrelidze, I., Shengelia, D., Tsutsunava, T., Chung, S.L., Yichiu, H., Chikhelidze, K., 2011. New data on the U-pb zircon age of the pre-alpine crystalline basement of the Black-Sea-central transcaucasian terrane and their geological significance. Bulletin of the Georgian National Academy of Sciences 5, 64–76.
Gärtner, A., Villeneuve, M., Linnemann, U., Gerdes, A., Youbi, N., Guillou, O., Rjimati, E.-C., 2016. History of the west african Neoproterozoic Ocean: key to the geotectonic history of circum-Atlantic peri-Gondwana (Adrar souttouf massif, moroccan Sahara). Gondw. Res. 29, 220–233.
Genç, Ş.C., Tüysüz, O., 2010. Tectonic setting of the jurassic bimodal magmatism in the Sakarya zone (central and Western pontides), northern Turkey: a geochemical and isotopic approach. Lithos 118 (1–2), 95–111.
Göncüoğlu, M.C., 2010. Introduction to the geology of Turkey: Geodynamic evolution of the pre-Alpine and Alpine Terranes. General Directorate of Mineral Research and Exploration (MTA), Ankara.
Göncüoğlu, M.C., Çimen, O., Gücer, M.A., Akal, C., Arslan, M., Simonetti, A., Karaoğlan, F., 2022. New Meso-and Neoproterozoic zircon U/Pb data from the crystalline basement of the Istanbul-Zonguldak Terrane in Safranbolu-Karadere area: A non-Gondwanan provenance?. Paper presented at 74th Geological Congress of Turkey with international participation at Ankara, Turkey.
Göncüoglu, M.C., Marroni, M., Sayit, K., Tekin, U.K., Ottria, G., Pandolfi, L., Elero, A., 2012. The aylı dağ ophiolite sequence (central-northern Turkey): a fragment of middle jurassic oceanic lithosphere within the intra-pontide suture zone. Ofioliti 37 (2), 77–92.
Göncüoglu, M.C., Marroni, M., Pandolfi, L., Ellero, A., Ottria, G., Catanzariti, R., Tekin, U.K., Sayit, K., 2014. The arkot dağ mélange in araç area, central Turkey: evidence of its origin within the geodynamic evolution of the intra-pontide suture zone. J. Asian Earth Sci. 85, 117–139.
Göncüoğlu, M.C., Turhan, N., Şentürk, K., Özcan, A., Uysal, Ş., Yaliniz, M.K., 2000. A geotraverse across northwestern Turkey: tectonic units of the Central Sakarya region and their tectonic evolution. Geol. Soc. Lond. Spec. Publ. 173 (1), 139–161.
Griffin, W.L., Belousova, E.A., Walters, S.G., O'Reilly, S.Y., 2006. Archaean and proterozoic crustal evolution in the eastern succession of the mt Isa district, Australia: U-pb and hf-isotope studies of detrital zircons *. Aust. J. Earth Sci. 53 (1), 125–149.
Grimes, C.B., John, B.E., Kelemen, P.B., Mazdab, F.K., Wooden, J.L., Cheadle, M.J., Hanghøj, K., Schwartz, J.J., 2007. Trace element chemistry of zircons from oceanic crust: a method for distinguishing detrital zircon provenance. Geology 35, 643–646.
Gücer, M.A., Arslan, M., Sherlock, S., Heaman, L.M., 2016. Permo-Carboniferous granitoids with jurassic high temperature metamorphism in central pontides, Northern Turkey. Mineralogy and Petrology 110 (6), 943–964.
Gücer, M.A., Arslan, M., Çimen, O., Sherlock, S.C., 2019. Petrology and 40Ar-39Ar dating of paragneisses from the devrekani massif (central pontides, northern Turkey): implications for the jurassic high-T metamorphism in an extensional tectonic environment. J. Asian Earth Sci. 181, 103888.
Gücer, M.A., 2014. Petrochemistry, petrology and geochronology of the Devrekani (Kastamonu, Turkey) metamorphics. Ph.D. thesis, Karadeniz Technical University (in Turkish with English abstract).
Horstwood, M.S.A., Košler, J., Gehrels, G., Jackson, S.E., McLean, N.M., Paton, C., Pearson, N.J., Sircombe, K., Sylvester, P., Vermeesch, P., Bowring, J.F., Condon, D.J., Schoene, B., 2016. Community-derived Standards for LA-ICP-MS U-(th-)pb geochronology - uncertainty propagation, age interpretation and data reporting. Geostand. Geoanal. Res. 40, 311–332.
Hoskin, P.W.O., Ireland, T.R., 2000. Rare earth element chemistry of zircon and its use as a provenance indicator. Geology 28 (7), 627.
Huang, Q., Neubauer, F., Liu, Y., Genser, J., Guan, Q., Chang, R., Yuan, S., Yu, S., 2022. Permian-triassic granites of the schladming complex (austroalpine basement): implications for subduction of the paleo-Tethys Ocean in the eastern Alps. Gondw. Res. 109, 205–224.
Karsli, O., Şengün, F., Dokuz, A., Kandemir, R., Aydin, F., Andersen, T., 2020. Silurian to Early devonian arc magmatism in the western Sakarya zone (NW Turkey), with inference to the closure of the Rheic Ocean. Lithos 370–371, 105641.
Karslıoğlu, Ö., Ustaömer, T., Robertson, A.H.F., Peytcheva, I., 2012. Age and provenance of detrital zircons from a sandstone turbidite of the Triassic-Early Jurassic Küre Complex, Central Pontides. Paper presented at International Earth Science Colloquium on the Aegean Region at İzmir, Turkey.
Kostrovitsky, S.I., Skuzovatov, S.Y., Yakovlev, D.A., Sun, J., Nasdala, L., Wu, F.Y., 2016. Age of the siberian craton crust beneath the northern kimberlite fields: insights to the craton evolution. Gondw. Res. 39, 365–385.
Kozur, H.W., Aydın, M., Demir, O., Yakar, H., Göncüoğlu, M.C., Kuru, F., 2000. New stratigraphic and palaeogeographic results from the palaeozoic and Early mesozoic of the middle pontides (northern Turkey) in the azdavay, devrekani, küre and Inebolu areas: implications for the Carboniferous-Early cretaceous geodynamic evolution and some related remarks to the Karakaya oceanic Rift Basin. Geologia Croatica 53 (2), 209–268.
Li, X.-H., Long, W.-G., Li, Q.-L., Liu, Y., Zheng, Y.-F., Yang, Y.-H., Chamberlain, K.R., Wan, D.-F., Guo, C.-H., Wang, X.-C., Tao, H., 2010. Penglai zircon megacrysts: a potential new working reference material for microbeam determination of Hf–O isotopes and U-pb age. Geostand. Geoanal. Res. 34 (2), 117–134.
Linnemann, U., Ouzegane, K., Drareni, A., Hofmann, M., Becker, S., Gärtner, A., Sagawe, A., 2011. Sands of West Gondwana: an archive of secular magmatism and plate interactions – a case study from the cambro-Ordovician section of the tassili ouan Ahaggar (algerian Sahara) using U-Pb–LA-ICP-MS detrital zircon ages. Lithos 123 (1–4), 188–203.
Löwen, K., Meinhold, G., Güngör, T., Berndt, J., 2017. Palaeotethys-related sediments of the Karaburun peninsula, western Turkey: constraints on provenance and

stratigraphy from detrital zircon geochronology. Int. J. Earth Sci. 106 (8), 2771–2796.
Ludwig, K.R., 2012. User's manual for isoplot version 3.75–4.15: a geochronological toolkit for Microsoft excel. Berkeley Geochronological Center Special Publication.
Marroni, M., Göncüoğlu, M.C., Frassi, C., Sayit, K., Pandolfi, L., Ellero, A., Ottria, G., 2020. The intra-pontide ophiolites in northern Turkey revisited: from birth to death of a neotethyan oceanic domain. Geosci. Front. 11, 129–149.
McLennan, S.M., Hemming, S., McDaniel, D.K., Hanson, G.N., 1993. Geochemical approaches to sedimentation, provenance, and tectonics. In: Johnsson, M.J., Basu, A. (Eds.), Processes Controlling the Composition of Clastic Sediments. Geological Society of America, pp. 21–40.
Mineral Research & Exploration General Directorate (MTA), 2002. Geological map series of Turkey, Ankara and Zonguldak geologic quadrangle map, scale 1:500.000 (in Turkish).
Nikishin, A.M., Ziegler, P.A., Abbott, D., Brunet, M.-F., Cloetingh, S., 2002. Permo-triassic intraplate magmatism and rifting in Eurasia: implications for mantle plumes and mantle dynamics. Tectonophysics 351 (1–2), 3–39.
Nzegge, O.M., 2008. Petrogenesis and geochronology of the deliktaş, sivrikaya and devrekani granitoids and basement, Kastamonu Belt-central pontides (NW Turkey): evidence for late paleozoic-mesozoic plutonism, and geodynamic interpretation. University of Tübingen. Ph.D. thesis.
Okay, A.I., Bozkurt, E., Satır, M., Yiğitbaş, E., Crowley, Q.G., Shang, C.K., 2008. Defining the southern margin of avalonia in the pontides: geochronological data from the late proterozoic and Ordovician granitoids from NW Turkey. Tectonophysics 461 (1–4), 252–264.
Okay, A.I., Altiner, D., Kiliç, A.M., 2015. Triassic limestone, turbidites and serpentinite–the Cimmeride orogeny in the central pontides. Geol. Mag. 152 (3), 460–479.
Okay, A.I., Altiner, D., Sunal, G., Aygül, M., Akdoğan, R., Altiner, S., Simmons, M., 2018. Geological evolution of the central pontides. Geol. Soc. Lond. Spec. Publ. 464 (1), 33–67.
Okay, A.I., Nikishin, A.M., 2015. Tectonic evolution of the southern margin of laurasia in the Black Sea region. Int. Geol. Rev. 57 (5–8), 1051–1076.
Okay, A., Satır, M., Tüysüz, O., Akyüz, S., Chen, F., 2001. The tectonics of the strandja massif: late-Variscan and mid-mesozoic deformation and metamorphism in the northern Aegean. Int. J. Earth Sci. 90 (2), 217–233.
Okay, A.I., Topuz, G., 2017. Variscan orogeny in the Black Sea region. Int. J. Earth Sci. 106 (2), 569–592.
Okay, A.I., Satır, M., Maluski, H., Siyako, M., Monie, P., Metzger, R., Akyüz, S., 1996. Paleo- and neo-tethyan events in northwest Turkey: geological and geochronological constraints. In: Yin, A., Harrison, M. (Eds.), The Tectonic Evolution of Asia. Cambridge University Press, pp. 420–441.
Okay, A.I., Sunal, G., Sherlock, S., Altıner, D., Tüysüz, O., Kylander-Clark, A.R.C., Aygül, M., 2013. Early cretaceous sedimentation and orogeny on the active margin of Eurasia: southern central pontides, Turkey. Tectonics 32 (5), 1247–1271.
Okay, A.I., Sunal, G., Tüysüz, O., Sherlock, S., Keskin, M., Kylander-Clark, A.R.C., 2014. Low-pressure-high-temperature metamorphism during extension in a jurassic magmatic arc, central pontides, Turkey. Journal of Metamorphic Geology 32 (1), 49–69.
Ondrejka, M., Uher, P., Putiš, M., Kohút, M., Broska, I., Larionov, A., Bojar, A.-V., Sobocký, T., 2021. Permian A-type granites of the Western Carpathians and transdanubian regions: products of the pangea supercontinent breakup. Int. J. Earth Sci. 110, 2133–2155.
Özbey, Z., Ustaömer, T., Robertson, A.H.F., Ustaömer, P.A., 2013. Tectonic significance of late Ordovician granitic magmatism and clastic sedimentation on the northern margin of Gondwana (tavşanlı zone, NW Turkey). J. Geol. Soc. London 170 (1), 159–173.
Özkan, M., Çelik, Ö.F., Soycan, H., Çörtük, R.M., Marzoli, A., 2020. The middle jurassic and Early cretaceous basalt-radiolarian chert association from the tekelidağ mélange, eastern İzmir-Ankara-Erzincan suture zone (northern Turkey). Cretac. Res. 107, 104280.
Pearce, J.A., Cann, J.R., 1973. Tectonic setting of basic volcanic rocks determined using trace element analyses. Earth Planet. Sci. Lett. 19 (2), 290–300.
Pearce, J.A., Peate, D.W., 1995. Tectonic implications of the composition of volcanic ARC magmas. Annu. Rev. Earth Planet. Sci. 23 (1), 251–285.
Robertson, A., Parlak, O., Ustaömer, T., Taslı, K., İnan, N., Dumitrica, P., Karaoğlan, F., 2014. Subduction, ophiolite genesis and collision history of tethys adjacent to the eurasian continental margin: new evidence from the eastern pontides, Turkey. Geodinamica Acta 26 (3–4), 230–293.
Robertson, A.H.F., Ustaömer, T., 2004. Tectonic evolution of the intra-pontide suture zone in the armutlu peninsula, NW Turkey. Tectonophysics 381 (1–4), 175–209.
Rubatto, D., 2002. Zircon trace element geochemistry: partitioning with garnet and the link between U-pb ages and metamorphism. Chem. Geol. 184 (1–2), 123–138.
Rudnick, R.L., Gao, S., 2003. Composition of the continental crust. In: Treatise on Geochemistry. Elsevier, pp. 1–64.
Saccani, E., 2015. A new method of discriminating different types of post-archean ophiolitic basalts and their tectonic significance using th-nb and ce-dy-yb systematics. Geosci. Front. 6 (4), 481–501.
Sapancı, Ö., Tokat, G., Eraslan, N.K., Karakaya, A.O., Gücer, M.A., Çimen, O., 2023. Geochemical and radiometric data for mafic rocks from the guleman ophiolite (SE, Turkey): new insights on the geodynamic evolution of the southern neo-Tethyan ocean. Lithos 442–443, 107071.
Seghedi, A., 2011. Palaeozoic formations from dobrogea and pre-dobrogea – an overview. Turk. J. Earth Sci. 21 (5), 669–721.
Şen, F., 2023. Ordovician arc and syncollisional magmatism in the İstanbul-Zonguldak tectonic unit (NW Turkey): implications for the consumption of the teisseyre-Tornquist Ocean in Far East avalonia. Mineral. Petrol. https://doi.org/10.1007/s00710-023-00812-7.
Şengör, A.M.C., Yilmaz, Y., 1981. Tethyan evolution of Turkey: a plate tectonic approach. Tectonophysics 75 (3–4), 181–241.
Sláma, J., Košler, J., Condon, D.J., Crowley, J.L., Gerdes, A., Hanchar, J.M., Horstwood, M.S.A., Morris, G.A., Nasdala, L., Norberg, N., Schaltegger, U., Schoene, B., Tubrett, M.N., Whitehouse, M.J., 2008. Plešovice zircon — a new natural reference material for U-pb and hf isotopic microanalysis. Chem. Geol. 249, 1–35.
Sun, S.-S., McDonough, W.F., 1989. Chemical and isotopic systematics of oceanic basalts: implications for mantle composition and processes. Geol. Soc. Lond. Spec. Publ. 42 (1), 313–345.
Sunal, G., 2012. Devonian magmatism in the western Sakarya zone, Karacabey region, NW Turkey. Geodinamica Acta 25 (3–4), 183–201.
Sunal, G., Natal'in, B.A., Satir, M., Toraman, E., 2006. Paleozoic magmatic events in the strandja massif, NW Turkey. Geodinamica Acta 19 (5), 283–300.
Topuz, G., Altherr, R., Siebel, W., Schwarz, W.H., Zack, T., Hasözbek, A., Barth, M., Satır, M., Şen, C., 2010. Carboniferous high-potassium I-type granitoid magmatism in the eastern pontides: the Gümüşhane pluton (NE Turkey). Lithos 116, 92–110.
Topuz, G., Candan, O., Okay, A.I., von Quadt, A., Othman, M., Zack, T., Wang, J., 2020. Silurian anorogenic basic and acidic magmatism in Northwest Turkey: implications for the opening of the paleo-tethys. Lithos 356–357, 105302.
Tüysüz, O., 1990. Tectonic evolution of a part of the tethyside orogenic collage: the Kargi massif, northern Turkey. Tectonics 9 (1), 141–160.
Ustaömer, P.A., Mundil, R., Renne, P.R., 2005. U/Pb and Pb/Pb zircon ages for arc-related intrusions of the Bolu massif (W pontides, NW Turkey): evidence for late precambrian (cadomian) age. Terra Nova 17 (3), 215–223.
Ustaömer, T., Robertson, A.H.F., 1999. Geochemical evidence used to test alternative plate tectonic models for pre-upper jurassic (palaeotethyan) units in the central pontides. N Turkey. Geological Journal 34 (1–2), 25–53.
Ustaömer, P.A., Ustaömer, T., Gerdes, A., Zulauf, G., 2011. Detrital zircon ages from a lower Ordovician quartzite of the İstanbul exotic terrane (NW Turkey): evidence for amazonian affinity. Int. J. Earth Sci. 100 (1), 23–41.
Ustaömer, P.A., Ustaömer, T., Robertson, A.H.F., 2012. Ion probe U-pb dating of the Central Sakarya basement: a peri-Gondwana terrane intruded by late lower Carboniferous subduction/ collision-related granitic rocks. Turk. J. Earth Sci. 21 (6), 905–932.
Ustaömer, T., Ustaömer, P.A., Robertson, A.H.F., Gerdes, A., 2016. Implications of U-pb and Lu–Hf isotopic analysis of detrital zircons for the depositional age, provenance and tectonic setting of the permian-triassic palaeotethyan Karakaya complex, NW Turkey. Int. J. Earth Sci. 105 (1), 7–38.
Wang, C., Liang, X., Foster, D.A., Fu, J., Jiang, Y., Dong, C., Zhou, Y., Wen, S., Van Quynh, P., 2016. Detrital zircon U-pb geochronology, Lu–Hf isotopes and REE geochemistry constrains on the provenance and tectonic setting of Indochina block in the paleozoic. Tectonophysics 677–678, 125–134.
Wiedenbeck, M., Allé, P., Corfu, F., Griffin, W.L., Meier, M., Oberli, F., Quadt, A.V., Roddick, J.C., Spiegel, W., 1995. Three natural zircon standards for U-th-pb, lu-hf, trace element and REE analyses. Geostand. Newslett. 19 (1), 1–23.
Wu, F.Y., Yang, Y.H., Xie, L.W., Yang, J.H., Xu, P., 2006. Hf isotopic compositions of the standard zircons and baddeleyites used in U-pb geochronology. Chem. Geol. 234 (1–2), 105–126.
Yılmaz, O., 1980. Daday-devrekani masifi kuzeydoğu kesimi litostratigrafi birimleri ve tektoniği. Yerbilimleri 5–6, 101–131 in Turkish with English abstract.
Yılmaz, O., Bonhomme, M.G., 1991. K-ar isotopic age evidence for a lower to middle jurassic low-pressure and a lower cretaceous high-pressure metamorphic events in north-central Turkey. Terra Abstracts 3, 501.
Yılmaz, İ., Şahin, S.Y., Aysal, N., Güngör, Y., Akgündüz, A., Bayhan, U.C., 2022. Geochronology, geochemistry and tectonic setting of the cadomian (Ediacaran–Cambrian) magmatism in the istranca (strandja) massif: new insights into magmatism along the northern margin of Gondwana in NW Turkey. Int. Geol. Rev. 64 (17), 2456–2477.
Yuan, H.L., Gao, S., Dai, M.N., Zong, C.L., Günther, D., Fontaine, G.H., Liu, X.M., Diwu, C.R., 2008. Simultaneous determinations of U-pb age, hf isotopes and trace element compositions of zircon by excimer laser-ablation quadrupole and multiple-collector ICP-MS. Chem. Geol. 247 (1–2), 100–118.
Yuan, S., Neubauer, F., Liu, Y., Genser, J., Liu, B., Yu, S., Chang, R., Guan, Q., 2020. Widespread permian granite magmatism in lower austroalpine units: significance for permian rifting in the eastern Alps. Swiss J. Geosci. 113 (1), 18.